Multiple PDZ Domain Protein Maintains Patterning of the Apical Cytoskeleton in Sensory Hair Cells

Amandine Jarysta[1], and Basile Tarchini[1,2,3#]

[1] The Jackson Laboratory, Bar Harbor, ME, 04609, USA

[2] Department of Medicine, Tufts University, Boston, 02111, MA, USA

[3] Graduate School of Biomedical Science and Engineering (GSBSE), University of Maine, Orono, 04469, ME, USA

Corresponding Author and Lead Contact: basile.tarchini@jax.org

Phone: 207-2886986

SUMMARY

Sound transduction occurs in the hair bundle, the apical compartment of sensory hair cells in the inner ear. The hair bundle is formed of stereocilia aligned in rows of graded heights. It was previously shown that the GNAI-GPSM2 complex is part of a developmental blueprint that defines the polarized organization of the apical cytoskeleton in hair cells, including stereocilia distribution and elongation. Here we report a novel and critical role for Multiple PDZ domain (MPDZ) protein during apical hair cell morphogenesis. We show that MPDZ is enriched at the hair cell apical membrane, and required there to maintain the proper segregation of apical blueprints proteins, including GNAI-GPSM2. Loss of the blueprint coincides with misaligned stereocilia in *Mpdz* mutants, and results in permanently misshapen hair bundles. Graded molecular and structural defects along the cochlea can explain the profile of hearing loss in *Mpdz* mutants, where deficits are most severe at high frequencies.

INTRODUCTION

Auditory function relies on the ability of sensory hair cells (HCs) in the auditory epithelium to detect sound vibrations. This is the role of the hair bundle, a highly organized brush of actin-based membrane protrusions, or stereocilia, located at the HC apical surface. Mutations affecting proteins involved in the morphogenesis or the maintenance of the hair bundle lead to hearing loss [1-4].

We and others showed that inhibitory Guanine nucleotide-binding proteins (G proteins) of the alpha family (GNAI1-3, collectively GNAI) bind the scaffold protein G Protein Signaling Modulator 2 (GPSM2) to form a complex essential for the polarized morphogenesis of the apical cytoskeleton in HCs [5-11]. Post-mitotic HCs are initially covered uniformly with microvilli, but planar polarized enrichment of GNAI-GPSM2 and Inscuteable (INSC) at the apical membrane defines a lateral/abneural region without protrusions, the bare zone [8]. GNAI-GPSM2 generates and expands the bare zone by antagonizing the polarity kinase aPKC that coincides with the microvillar HC surface. Complementary GNAI-GPSM2 vs aPKC distribution thus forms an apical blueprint that defines the lateral edge of the emerging hair bundle when microvilli grow into stereocilia [8]. As HCs mature, the GNAI-GPSM2 complex is then trafficked to the tips of stereocilia adjacent to the bare zone by the MYO15A motor [7, 9, 10]. At stereocilia tips, GNAI-GPSM2 promotes enrichment of MYO15A and other partners, conferring the first stereocilia row with its unique tallest identity [10]. Loss of GNAI or GPSM2 in mouse leads to stereocilia stunting, and the resulting immature hair bundle morphology in adults coincides with profound deafness [5, 7, 9]. In humans, mutations in *GPSM2* are responsible for the Chudley-McCullough syndrome where hearing loss is the principal affliction [12, 13].

GNAI-GPSM2 is enriched and polarized independently from planar cell polarity (PCP) proteins [6, 8], the machinery that regulates HC orientation via intercellular communication at apical cell-cell junctions [14, 15]. Accordingly, polarization of a subset of PCP proteins was recently proposed to depend on Wnt secretion, but severely

disrupted cochlear elongation and morphogenesis in *Wntless* (*Wls*) mutants left GNAI-GPSM2 enrichment intact at the HC surface [16, 17]. Similarly, polarized segregation of GNAI-GPSM2 and aPKC was preserved in mutants lacking other polarity proteins that occupy the lateral apical HC junction: DAPLE/CCDC88C [18] and PARD3 [19]. It thus remains unclear how GNAI-GPSM2 is first polarized and then maintained at the HC apical membrane. Here, we hypothesized that GNAI-GPSM2 might more specifically interact with polarity proteins that occupy the HC apical membrane. To find possible candidates, we investigated proteins well-known to establish apico-basal polarization in other epithelial systems.

Multiple PDZ domain (MPDZ, or MUPP1) is a large adapter protein with 13 PDZ (PSD95/DLG1/ZO1) domains that mediates protein-protein interactions and was first reported as interacting with the HTR2C serotonin receptor [20, 21]. MPDZ is a scaffold protein that clusters binding partners in defined cell compartments, for example SynGAP and CaMKII at synapses [22], as well as Delta Like protein 1 and 4 (DLL1/4) and Nectin-2 at epithelial apical junctions [23]. MPDZ is a paralog of INADL/PATJ, a scaffolding protein that binds MPP5/PALS1, which in turn binds the integral protein CRB3 to form the Crumbs complex [24-27]. The Crumbs complex plays a highly conserved role in the establishment of epithelial apico-basal polarity [28, 29], including the formation of tight junctions in mammals [26, 27, 30-33]. MPDZ itself was reported as a component of tight junctions, and MPDZ can directly bind Claudins [34-36] as well as many of the INADL partners, including JAM1 [35, 37] and ZO1 [37]. Interestingly, like INADL, MPDZ can bind MPP5 to form an alternative Crumbs complex (CRB3-MPP5-MPDZ) with distinct cellular functions from the better-described CRB3-MPP5-INADL complex [27, 37]. Recently, MPDZ was shown to bind and cooperate with DAPLE at apical junctions for apical cell constriction in cell culture and during neurulation [38, 39].

In human and mice, mutations in *MPDZ* lead to multiple ependymal malformations that compromise the lining of the brain ventricles [40, 41]. These defects were initially proposed to result from defective ependymal tight junctions, but a recent study also uncovered a more specific role for MPDZ in the choroid plexus that secretes

92 cerebrospinal fluid into the ventricles [42]. Interestingly, although barrier integrity was
93 defective in both organs, MPDZ was only reported as apical in choroid plexus epithelial
94 cells, and not visibly enriched at tight junctions [42]. Likely due to ependymal and/or
95 choroid plexus dysfunction, *MPDZ* is one of the few genes linked to congenital
96 hydrocephalus in humans [40, 43-45] and mice [41, 42]. Of note, a young patient carrying
97 two distinct *MPDZ* mutations in *trans* also presented with sensorineural hearing loss,
98 suggesting a potential role for MPDZ in the inner ear [45].
99
100 In this study, we identify a new function for MPDZ during HCs development. Surprisingly,
101 MPDZ is not detected at apical cell junctions in the auditory epithelium, but at the HC
102 apical membrane where it co-localizes with MPP5 and CRB3. We show that MPDZ is
103 necessary to maintain the apical segregation of GNAI-GPSM2 and aPKC. Loss of this
104 apical blueprint in *Mpdz* mutants coincides with misaligned stereocilia and dysmorphic
105 hair bundles. Molecular and morphological defects persist in young adults and are likely
106 responsible for severe hearing loss in *Mpdz* mutants.
107

108 RESULTS

109

110 **MPDZ occupies the hair cell apical membrane with a lateral bias**

111

112 To investigate a potential role for MPDZ in the auditory epithelium, we started by
113 immunolabeling MPDZ at different developmental stages with a validated antibody
114 targeting the third PDZ domain (PDZ3) [34]. As early as embryonic day (E) 17.5, MPDZ
115 signal was obvious at the HC apex, spanning most of the apical membrane (Fig. 1A).
116 MPDZ was most highly enriched at the bare zone, the flat region deprived of protrusions
117 lying lateral to the tallest stereocilia [8]. MPDZ signal was lower on the medial side of the
118 hair bundle, and absent or barely detectable at the position of the hair bundle itself. A
119 similar MPDZ enrichment pattern was observed in neonate HCs at postnatal day (P) 0
120 and P4 (Fig. 1A). Of note, INSC, GNAI and GPSM2 are by contrast strictly enriched at
121 the bare zone and are thus more obviously planar polarized than MPDZ [6, 8, 11].

122

123 **Loss of MPDZ results in apical defects in developing hair cells**

124

125 We obtained a constitutive *Mpdz* mouse mutant from the IMPC repository (C57BL/6N-
126 *Mpdz*$^{em1(IMPC)J}$/Mmucd, hereafter *Mpdz*^{DEL}). This strain carries an indel in *Mpdz* exon 6
127 which is predicted to cause a frameshift resulting in an early truncation of the protein after
128 the first of 13 PDZ domains. We did not observe lethality in *Mpdz*$^{DEL/DEL}$ animals, whereas
129 previous *Mpdz* mutants died around 3-4 week of age (see Supplementary Table 1) [41,
130 42, 46]. Nevertheless, as expected, MPDZ antibody signal was entirely missing in the
131 *Mpdz*$^{DEL/DEL}$ auditory epithelium, establishing this strain as a proper loss-of-function model
132 in HCs (Fig. 1A).

133

134 Based on its localization, we asked whether MPDZ could be involved in apical HC
135 morphogenesis. We first imaged the hair bundle at embryonic and postnatal stages using
136 conjugated phalloidin to reveal F-actin. At E17.5, stereocilia organization appeared
137 comparable between *Mpdz* mutants and littermate controls at the cochlear base (Fig. 1B).
138 By birth (P0) however and at P4, apical HC defects were obvious in outer HCs (OHCs),

where hair bundles lacked their characteristic V-shape and were frequently split (Fig. 1B). Because 3-dimensional organization of protruding stereocilia can be confusing in flat-mounts, we labeled stereocilia rootlets at P6 with an antibody against TRIOBP [47]. We found that stereocilia were severely misaligned in *Mpdz* mutants (Fig. 1C). Stereocilia also formed incomplete supernumerary rows most obvious on the lateral side of the bundle at P6 (Fig. 1C, arrowhead). Inner HCs (IHCs) showed similar, but milder defects from P0 (Fig. 1B-C). Together, these results suggest that MPDZ acts at the apical membrane outside of the forming hair bundle and is important for the proper localization and cohesive, arrayed organization of stereocilia in postnatal HCs.

Labeling of apical junctions with ZO1 revealed an abnormally round and possibly reduced OHC circumference in P4 *Mpdz* mutants compared to control littermates (Fig. 1D). IHCs were not visibly affected. We quantified the apical surface area in OHCs and observed a significant reduction in *Mpdz* mutants at the cochlear base and apex at P4, but not at P0 (Fig. 1E). The OHC apical surface is known to decrease after P0 along with a remodeling of the cell circumference that closely mirrors hair bundle development [48]. MPDZ might thus regulate this process at the flat apical membrane, impacting both the placement of stereocilia and the shape of the HC junctions. GNAI and GPSM2 share MPDZ localization at the bare zone, and are also essential to define the lateral outline of the forming hair bundle [6, 8, 11], as well as the asymmetry of height and identities across stereocilia rows [7, 9, 10]. Next, we thus analyzed how GNAI-GPSM2 localized in *Mpdz* mutants.

Loss of MPDZ causes a progressive delocalization of GNAI-GPSM2 at the hair cell surface

We assessed GNAI localization in HCs in the first postnatal week. At P2, GNAI was distributed normally in *Mpdz* mutant HCs along the whole cochlea (Fig. 2A). In contrast, at P4 many OHCs at the cochlear base showed medial delocalization of GNAI, whereas HCs at mid and apex cochlear positions retained normal GNAI distribution. At P7, all OHCs at the base and many OHCs at the mid position showed delocalized GNAI, and HCs at the apex retained normal GNAI distribution. We conclude that loss of MPDZ

170 progressively alters apical GNAI distribution as HC differentiation progresses in time and
171 spatially along a cochlear apex to base gradient [49]. Quantification of GNAI signal
172 intensity in P4 OHCs confirmed a drastic delocalization from the lateral to the medial side
173 of the hair bundle. Compared to control littermates, GNAI enrichment at the lateral bare
174 zone decreased, and medial GNAI enrichment increased in *Mpdz* mutants (Fig. 2B).
175
176 We next attempted to define more precisely how GNAI was redistributed in *Mpdz* mutant
177 HCs. In P4 mutants OHCs at the base, GNAI was variably depleted at the bare zone and
178 at stereocilia tips, and was instead ectopically found 1) on the longitudinal or medial sides
179 of the hair bundle (Fig. 2C; arrows), and 2) at the medial HC junction with the neighboring
180 support cell labeled with Afadin/AFDN (Fig. 2C; hollow arrowheads). Interestingly, GNAI
181 was consistently missing at the center of the bare zone, whereas it was often retained at
182 the bare zone periphery in *Mpdz* mutants. We quantified this trend by measuring GNAI
183 enrichment in 3 equal sub-regions of the bare zone along the longitudinal axis (Fig. 2D).
184 GNAI signals were equal in all sub-regions in control animals, as expected based on
185 uniform GNAI enrichment across the bare zone. In contrast, *Mpdz* mutants showed a
186 significant GNAI decrease in the central (b) compared to the peripheral sub-regions (a, c)
187 (Fig. 2D). These results suggest that GNAI may be first lost centrally near the basal body,
188 and invading the medial apical membrane by “seeping” through the sides of the hair
189 bundle.
190
191 Interestingly, GNAI presence or absence at stereocilia tips coincided spatially with GNAI
192 presence or absence at the adjacent portion of the bare zone in single OHCs (Fig. 2E).
193 When GNAI was only maintained at the bare zone periphery (white arrow), GNAI was
194 only maintained at the tips of peripheral stereocilia in the hair bundle (Fig. 2E, white
195 arrowhead). Complete medial relocalization of GNAI outside the hair bundle (orange
196 arrow) was paired with an almost complete loss of GNAI at tips. GNAI-GPSM2 enrichment
197 at the bare zone is progressively reduced during HC maturation [8]. Low amounts of GNAI
198 at the bare zone in P4 IHCs made delocalization to the flat surface and pairing with
199 outcomes at tips challenging to assess in IHCs. We did however observe reduced GNAI
200 bare zone enrichment in *Mpdz* mutant IHCs compared to controls, and a similar but less

severe loss of GNAI at stereocilia tips compared to OHCs (Fig. 2E). Spatial pairing of GNAI between HC compartments in *Mpdz* mutants supports our working model where prior GNAI-GPSM2 enrichment at the bare zone instructs its selective trafficking to adjacent stereocilia in the first row [9, 10].

Because disrupted hair bundle morphology obscured hair bundle orientation in *Mpdz* mutants, we next immunolabeled the kinocilium at P4. As in control HCs, the kinocilium was systematically located on the lateral side of the hair bundle in *Mpdz* mutants (Fig. 2F, arrowheads). This clarifies that progressive delocalization of GNAI to the medial apex is not indicating a change in HC orientation. As expected, the GNAI binding partner GPSM2 followed GNAI delocalization in *Mpdz* mutants (Fig. 2G).

The hair cell apical blueprint is globally disrupted in absence of MPDZ

INSC-GNAI-GPSM2 at the bare zone antagonizes aPKC at the medial apical surface, and the boundary between these two apical membrane compartments coincides with the lateral edge of the forming hair bundle [6, 8, 11]. Similar to GNAI and GPSM2, aPKC lost its spatial restriction in *Mpdz* mutants. At the cochlear base at P4, aPKC was restricted to the medial HC apex in control OHCs and IHCs, but ectopically found across the whole apical surface in *Mpdz* mutants (Fig. 3A). Measuring aPKC enrichment on each side of the hair bundle confirmed that the ratio between the lateral bare zone and the medial side was significantly higher in mutants compared to controls (Fig. 3B). This reflects an increase of aPKC intensity at the bare zone and a decrease at the medial side (see Supp. Data File). Of note, ectopic aPKC was previously reported upon *Gnai* and *Gpsm2* inactivation [6, 8], suggesting that aPKC invasion of the lateral apex in *Mpdz* mutants might be secondary to the downregulation of GNAI-GPSM2 there (Fig. 2). In contrast, aPKC was restricted medially as in control HCs at the cochlear apex at P4 (Fig. 3C), and along the whole cochlea at P0 (not shown).

Altogether, our results demonstrate that MPDZ is essential to maintain properly polarized and segregated GNAI-GPSM2 and aPKC domains in maturing HCs after P4. Delocalized

232 GNAI-GPSM2 enrichment at the flat HC surface and its corresponding loss at stereocilia
233 tips likely contribute to disrupted stereocilia alignment and generally dysmorphic hair
234 bundles (Fig. 1-C).
235
236 **MPDZ defines a Crumbs complex at the apical membrane in hair cells and choroid**
237 **plexus cells**
238
239 MPDZ was previously reported to localize and function at tight junctions in epithelial cells
240 [23, 35, 37]. Instead, our results revealed a role for MPDZ at the HC apical membrane,
241 past the apical junction separating HCs from their support cell neighbors. MPDZ is a
242 paralog of INADL/PATJ [37], a member of the CRB3-MPP5/PALS1-INADL Crumbs
243 complex well known to regulate epithelial development and apico-basal polarization [26,
244 32, 33, 50]. We next compared the localization of MPDZ and other Crumbs complex
245 members in neonate HCs using ZO1 as marker for apical junctions, and surface (XY) and
246 projection views (XZ) of confocal stacks.
247
248 At P0 and P4, MPP5 was most highly enriched at the bare zone but also detected medially
249 with little signal at the hair bundle (Fig. 4A), a distribution virtually identical to MPDZ (Fig.
250 1A). In addition, MPP5 was also detected at the HC apical junction (Fig. 4A, arrowhead).
251 Projection views confirmed that MPP5, but not MPDZ, colocalized with ZO1 at OHC-
252 support cell junctions (Fig. 4B, arrowheads). Occasional fixation artifacts separating the
253 plasma membrane of HCs and neighboring support cells suggested that MPP5 was
254 junctional in both cell types (Supp. Fig. 1A), as also expected from junctional MPP5
255 distribution at support cell-support cell contacts and outside the auditory epithelium (Fig.
256 4A). We tested multiple antibodies and protocols to immunolabel CRB3, the small integral
257 member of the Crumbs complex. After repeated failures, we obtained decent results using
258 an antibody against an intracellular CRB3 epitope and antigen retrieval with urea [51].
259 We observed CRB3 signal at the bare zone and at apical junctions, as for MPP5 (Fig.
260 4C). In contrast to other members of the Crumbs complex, INADL was not detected at
261 the HC apical membrane or at the HC apical junction (Fig. 4D), and appeared instead
262 limited to the apical junction of support cells (Supp. Fig. 1B). Together, these results

263 suggest that a MPDZ-MPP5-CRB3 complex specifically occupies the HC apical
264 membrane.
265
266 Unlike MPDZ, MPP5-CRB3 distribution also included apical junctions in HCs, and loss of
267 MPDZ was proposed to disrupt barrier integrity in ependymal and choroid plexus cells in
268 part by compromising tight junctions [41, 42]. We thus immunolabeled the choroid plexus
269 (4th ventricle) in P13-P15 wild-type mice. Interestingly, we found that, as in the auditory
270 epithelium, MPDZ was absent at ZO1-positive cell junctions but found at the apical
271 membrane with higher enrichment near the junctions (Supp. Fig. 2A, E). In contrast,
272 MPP5 and CRB3 were clearly detected at apical junctions in addition to the apical
273 membrane, as in HCs (Supp. Fig. 2B-C). INADL was not detected at all (Supp. Fig. D).
274 We conclude that in auditory and choroid plexus epithelial cells at least, MPDZ-MPP5-
275 CRB3 represents a Crumbs complex specifically addressed to the apical membrane.
276 MPP5-CRB3 also occupies apical junctions, potentially with another partner.
277
278 **MPDZ anchors MPP5 and CRB3 at the hair cell apex**
279
280 MPDZ is expected to function as an anchor for partner proteins carrying a PDZ-binding
281 domain, and MPDZ and MPP5 are known to interact directly [37, 52]. We wondered
282 whether the loss of MPDZ would disrupt Crumbs complex partners in addition to GNAI-
283 GPSM2 (Fig. 2) and aPKC (Fig. 3). At P0, MPP5 was missing at the bare zone in *Mpdz*
284 mutants, and apparently ectopically found in the hair bundle (Fig. 4E; solid arrowhead).
285 Measuring MPP5 intensity ratio between the bare zone and the hair bundle confirmed this
286 striking redistribution in *Mpdz* mutants (Fig. 4F). In contrast, MPP5 was still enriched at
287 HC junctions in *Mpdz* mutants (Fig. 4E; hollow arrowheads), in line with our inability to
288 detect MPDZ at junctions (Fig. 4B). Measuring MPP5 junctional signal revealed a modest
289 reduction in *Mpdz* mutants (Fig. 4G), but this could reflect the difficulty to quantify
290 junctional signals without including signals at the adjacent apical membrane. Similarly,
291 we observed that CRB3 signal was lost at the bare zone and ectopically found in the hair
292 bundle in P0 *Mpdz* mutants (Supp. Fig. 1C). As expected from its localization at support
293 cell junctions, INADL was unchanged in *Mpdz* mutants (Supp. Fig. 1D).

294

295 As we observed earlier disruption of MPP5 and CRB3 (P0) than GNAI-GPSM2 and aPKC
296 (P4) in *Mpdz* mutants, we conclude that MPDZ is directly required to anchor its Crumbs
297 complex partners MPP5-CRB3 at the HC apical membrane. In turn, loss of the Crumbs
298 complex at the flat apical membrane disrupts the polarization and segregation of GNAI-
299 GPSM2 and aPKC.

300

301 **GNAI-GPSM2 and MPDZ-MPP5 influence each other at the hair cell apical**
302 **membrane**

303

304 MPDZ is required to maintain the lateral polarization of GNAI-GPSM2 at the apical
305 membrane from P4 (Fig. 2), and MPDZ-MPP5-CRB3 is more highly enriched at the bare
306 zone compared to the medial HC surface (Fig. 1A, Fig. 4A, C). We thus reasoned that,
307 reciprocally, GNAI-GPSM2 might influence the distribution of MPDZ and MPP5 by
308 increasing their accumulation at the bare zone. To test this prediction, we analyzed a
309 constitutive *Gpsm2* mutant (*Gpsm2*^{DEL}) [8] and we globally downregulated GNAI activity
310 in HCs by expressing the catalytic subunit of Pertussis toxin (PTXa) with *Atoh1-Cre* [9].
311 At P4, *Gpsm2* mutant HCs lost preferential MPDZ enrichment at the bare zone (Fig. 5A).
312 Measuring the ratio of signal intensity on the medial versus lateral side of the hair bundle
313 confirmed a more uniform MPDZ distribution across the apical surface upon loss of
314 GPSM2 (Fig. 5B). Surprisingly however, these quantifications also revealed that MPDZ
315 signal intensity actually increased both on the medial and lateral sides in *Mpdz* mutants,
316 only more drastically on the medial side (Fig. 5C).

317

318 Relatedly, we observed more uniform MPDZ distribution across the HC apex in PTXa-
319 expressing HCs at P4 (Fig. 5D). Of note, PTXa provokes severe defects in OHC
320 orientation [8, 9], and consequently the bare zone was no longer systematically on the
321 lateral side of the auditory epithelium. We next immunolabeled MPP5 in *Gpsm2* and PTXa
322 mutants since MPP5 binds [37, 52] and co-localized with MPDZ at the HC surface. As
323 with MPDZ, preferential MPP5 enrichment at the bare zone was abolished in *Gpsm2* (Fig.
324 4E) and PTXa (Fig. 5F) mutant HCs at P4. Altogether, our results suggest that reciprocal

interactions between MPDZ-MPP5 and GNAI-GPSM2 ensure that proper amounts of each protein complex are maintained at the bare zone. Increased MPDZ enrichment on both sides of the hair bundle in absence of GPSM2 may indicate that GNAI-GPSM2 somehow limits the total amount of MPDZ allowed to occupy the apical membrane.

Progressive loss of the apical blueprint coincides with severe hair bundle defects and hearing loss in mature hair cells

Early loss of GNAI and GPSM2 in postmitotic HCs leads to hair bundle disorganization, stereocilia stunting and profound hearing loss in young adults [5, 7, 9, 10]. We asked how loss of MPDZ that provokes a later disruption of GNAI-GPSM2 (Fig. 2) impacts the auditory organ near maturity. At P21, we did not observe OHC or IHC death along the cochlea in *Mpdz* mutants based on MYO6 immunolabeling (Fig. 6A). This verifies that delocalized GNAI-GPSM2 and aPKC starting at P4 (Fig. 2-3) is not an indirect consequence of HC degeneration, but an active process.

GNAI delocalization in *Mpdz* mutants progresses from the cochlear base to the apex along with HCs differentiation (Fig. 2A). We immunolabeled GNAI at P15 to determine how this defect progresses beyond P7 (Fig. 2A). At the cochlear base, GNAI signal was visible at stereocilia tips in controls, but largely absent in mutant OHCs (Fig. 6B). In contrast, GNAI could be observed at stereocilia tips in both control and mutant OHCs at the cochlear apex (Fig. 6B). We conclude that variable loss of GNAI at stereocilia tips at P4 (Fig. 2E) evolves into a complete loss with time, and that the GNAI delocalization wave (Fig. 2A) never reaches the apex of the cochlea in *Mpdz* mutants. In P15 IHCs, GNAI signal at stereocilia tips was still largely visible both at the cochlear base and apex in *Mpdz* mutants (Fig. 6B). This suggests that the milder GNAI disruption observed at P4 in IHCs (Fig. 2E) does not evolve much by P15, or perhaps that GNAI trafficking to IHC tips is only delayed in *Mpdz* mutants.

To better resolve the hair bundle structure, we performed scanning electron microscopy (SEM) at P21. At the cochlear base, mutant OHCs retained a flattened hair bundle and

356 apical surface circumference (Fig. 6C), as seen in neonates (Fig. 1B). Mutant IHCs were
357 less affected but showed irregular stereocilia placement (Fig. 6C). At the cochlear apex
358 by contrast, OHC and IHC morphology was relatively normal, in line with normal
359 localization of GNAI at the bare zone (P7, Fig. 2A) and stereocilia tips (P15, Fig. 6B).
360
361 To pair morphological alterations with organ function, we recorded Auditory Brainstem
362 Response (ABR) in 4 week-old *Mpdz* mutants and control littermates. We presented
363 anesthetized animals with pure tone stimuli of variable sound pressure intensities (dB) to
364 record ABR waveforms with a subcutaneous probe (Fig. 6D). Plotting ABR thresholds
365 (Fig. 6D, arrowheads) by frequency and genotype revealed severe global hearing defect
366 in *Mpdz* mutants (Fig. 6E). At high frequencies (32 and 40 kHz), *Mpdz* mutants showed
367 complete hearing loss, with virtually no response to even the loudest stimuli (90dB). At
368 lower frequencies (8 and 16 kHz), *Mpdz* mutants did respond, but with a significantly
369 higher threshold compared to control littermates. More severe hearing loss at higher
370 frequencies was expected based on the tonotopic organization of HC frequency
371 sensitivity along the cochlear duct. HCs at the cochlear apex, less affected in *Mpdz*
372 mutants, detect lower frequencies.
373
374

375 DISCUSSION

376

377 We show that the polarity protein MPDZ is required to anchor a version of the Crumbs
378 complex (MPDZ-MPP5-CRB3) at the HC apical membrane. Loss of MPDZ (and
379 concomitant defects in MPP5-CRB3 apical enrichment) disrupts the maintenance of
380 GNAI-GPSM2 and aPKC in their polarized and segregated apical domains. Blurring of
381 this molecular blueprint must contribute to stereocilia misalignment and dysmorphic hair
382 bundles in *Mpdz* mutants, as similar defects were reported in absence of GNAI or
383 GPSM2. In turn, defective hair bundle morphogenesis is probably a leading cause for
384 hearing loss in *Mpdz* mutants.

385

386 In absence of MPDZ, hair bundle defects are visible at birth already, whereas defects in
387 the GNAI-GPSM2 vs aPKC apical blueprint and OHC circumference are only noted from
388 P4. While delocalization of GNAI-GPSM2 is likely an important contributing factor, loss of
389 MPDZ must interfere with other proteins required for early hair bundle development.
390 Interestingly, *Mpdz* mutant HCs show a striking relocalization of both MPP5 and CRB3
391 from the flat HC apex to the hair bundle at P0 (Fig. 4E; Supp. Fig. 1C). CRB3 was shown
392 to interact with actin-binding proteins including EPS8 [53] and Ezrin [33]. It is thus possible
393 that ectopic MPP5-CRB3 presence in growing stereocilia interferes with F-actin assembly
394 or with the association between F-actin and the plasma membrane, for example.

395

396 Of note, progressive delocalization of GNAI-GPSM2 and aPKC at the HC apical
397 membrane was previously reported in mutant HCs lacking the SMARCA4/BRG1 subunit
398 of the SWI/SNF chromatin remodeling complex [54]. Loss of SMARCA4 protein between
399 P1- P4 caused HCs to start dying from P8 however, questioning whether loss of protein
400 polarization at the HC apical membrane might possibly be a side effect of cellular decline.
401 In contrast to SMARCA4, loss of MPDZ does not lead to gross epithelial disorganization,
402 and all HCs survive at least until P21. Maintaining the molecular blueprint that regulates
403 cytoskeleton distribution at the HC surface is thus an active process. This conclusion is
404 supported by another recent study where disrupting proteostasis in postnatal HCs also
405 affected the polarized distribution of blueprint proteins in absence of HC death [55].

406

407 *Mpdz* is one of few genes associated with congenital hydrocephalus, and two studies
408 inactivating *Mpdz* in mouse reported severe hydrocephalus from P3 that proved lethal
409 before, or around 3 weeks of life [41, 42]. The mouse models analyzed were a gene-trap
410 allele in intron 11-12 [41, 42, 46] and a conditional deletion of exons 4-5 [41], both
411 expected to produce a loss-of-function. Intriguingly, we do not observe hydrocephalus in
412 $Mpdz^{DEL/DEL}$ mutants produced by the KOMP consortium (C57BL/6N-
413 $Mpdz^{em1(IMPC)J}$/Mmucd), where an indel in exon 6 is expected to truncate the protein after
414 the first of 13 PDZ domains. We observed a sub-mendelian frequency of homozygotes
415 before weaning age, but we could obtain and breed $Mpdz^{DEL/DEL}$ adults of both sexes
416 (43% of progeny from $Mpdz^{DEL/DEL}$ x $Mpdz^{DEL/+}$ was homozygote; see Supp. Table 1 for a
417 comparison between *Mpdz* alleles). The cause of this discrepancy is unclear, but may
418 involve differences in genetic background between the C57BL6/J and C57BL6/N strains.
419 Study of another gene linked to congenital hydrocephalus, *L1cam*, revealed a potent
420 modifier locus on chromosome 5 [56]. Importantly, we use a validated MPDZ antibody
421 [34] that showed a loss of signal in the choroid plexus of gene-trap *Mpdz* mutants [42]. A
422 similar absence of signal in $Mpdz^{DEL/DEL}$ HCs (Figure 1A) thus validates the KOMP allele
423 as a bona fide loss-of-function. This conclusion is reinforced by severe morphological and
424 auditory defects in $Mpdz^{DEL/DEL}$ mutants.

425

426 Interestingly, MPDZ is limited to the apical membrane in HCs and choroid plexus epithelial
427 cells, and could not be detected along with MPP5-CRB3 at apical junctions. Loss of MPDZ
428 does however affect the structure of apical junctions in choroid plexus epithelial cells [42],
429 and the circumference of OHCs in the auditory epithelium (Fig. 1D-E). The latter might be
430 an indirect consequence where hair bundle defects affect HC junction remodeling [48],
431 but it is not unexpected that apical membrane proteins in the vicinity of tight junctions
432 would participate in the establishment and maintenance of junctional integrity. In fact, a
433 recent study identified the Crumbs complex (INADL-MPP5-CRB3) as defining a transition
434 zone between tight junctions and the free apical membrane, which the authors coined as
435 the ‘vertebrate marginal zone’ [57].

436

437

438 In other contexts by contrast, MPDZ was reported as enriched at apical junctions [23, 35,
439 37-39]. For example, the G protein regulator DAPLE and MPDZ co-localize and cooperate
440 at junctions during apical cell constriction in cultured cell monolayers and in
441 neuroepithelial cells [38, 39]. Moreover, *DAPLE* is with *MPDZ* one of a few genes linked
442 to congenital hydrocephalus in human and mice [58-60]. In auditory HCs however,
443 DAPLE is enriched laterally at the apical HC junction [18], a distinct distribution from
444 MPDZ at the HC apical membrane. In addition, apical HC defects in *Daple* mutants are
445 more severe and distinct from the ones we report here in *Mpdz* mutants [18]. We thus
446 conclude that the epithelial cell context must dictate what binding partners and subcellular
447 compartment MPDZ adopts.
448

449 In summary, our results show that MPDZ specifically patterns the HC apical membrane,
450 in part by maintaining the proper planar segregation of blueprint proteins at neonate
451 stages. Loss of MPDZ leads to permanent hair bundle disorganization that is likely the
452 etiology of severe hearing loss in young adults.
453
454
455
456
457

ACKNOWLEDGMENTS

We are particularly grateful to Dr. Elior Peles (Weizmann Institute of Science) for sharing the MPDZ antibody, and to Dr. Xaralabos Varelas (Boston University) for sharing the CRB3 antibody. The *Mpdz* mouse model was produced by the KOMP program led by Steve Murray at The Jackson Laboratory, and was shared by the group of Patsy Nishina. A.J. was supported by a 2-year postdoctoral fellowship from Fondation pour l'Audition, Paris, France (FPA RD2018-3). This work was supported by the National Institute on Deafness and Other Communication Disorders with R01 DC015242 and DC018394 to B.T.

AUTHOR CONTRIBUTION

B.T conceived the study. A.J and B.T. designed, and A.J performed and analyzed all experiments. B.T. and A.J. wrote the manuscript, B.T. secured funding.

COMPETING INTERESTS

The authors declare no competing interests.

DATA AVAILABILITY STATEMENT

All data generated or analyzed in this study are included in this published article (and its supplementary information file).

483 METHODS

484

485 **Mice**

486

487 The *Mpdz*^{DEL} strain (C57BL/6N-*Mpdz*$^{em1(IMPC)J}$/Mmucd, MGI: 5571597) was produced by
488 the KnockOut Mouse Project Consortium (KOMP) at The Jackson Laboratory. *Gpsm2*^{DEL}
489 *(Gpsm2*$^{tm1a(EUCOMM)Wtsi}$; MGI:4441912 [8]) and *R26-loxP-stop-loxP-mycPTXa* (*Gt*
490 *(ROSA)26Sor*$^{em1(ptxA)Btar}$; MGI:6163665 [9]) were described previously. Wild-type samples
491 analyzed were in a mixed genetic background (C57BL/6J x FVB/NJ). Mouse samples
492 analyzed ranged in age from E17.5 to 4-week old as indicated in each figure, and included
493 both males and females. Heterozygote *Mpdz*$^{DEL/+}$ animals did not exhibit morphological,
494 molecular or hearing defects, and were thus systematically used as littermate controls for
495 *Mpdz*$^{DEL/DEL}$ mutants to reduce the number of animals produced for the study. Animals
496 were maintained under standard housing and all animal work was reviewed for
497 compliance and approved by the Animal Care and Use Committee of The Jackson
498 Laboratory.

499

500 **Immunofluorescence and antibodies**

501

502 For embryonic and neonate stages, temporal bones were isolated and either immediately
503 micro-dissected to expose the sensory epithelium before fixing in paraformaldehyde (PFA
504 4%) for 1h at 4°C, or incubated in trichloroacetic acid (TCA 10%) for 10min on ice before
505 dissection, depending on the antibodies used (indicated below). After rinsing with PBS,
506 the tectorial membrane was removed, and samples were blocked and permeabilized in
507 PBS with 0.5% Triton-X100 and bovine serum albumin (1%) for at least 1h at room
508 temperature before application of the primary antibodies. For CRB3 labeling, we used the
509 following antigen retrieval procedure: the postnatal inner ear was fixed before micro-
510 dissection for 1h at room temperature in PFA. The auditory epithelium was then exposed,
511 blocked and permeabilized as above for 20 minutes, and the incubated in urea (0.8M) for
512 1h at 50°C, then for 20 minutes at 65°C.

513 For postnatal stages after P7, temporal bones were isolated and the cochlea punctured
514 at the apex to facilitate access of the fixative before immersion fixation in
515 paraformaldehyde (PFA 4%) for 1h at 4°C or room temperature. After rinsing with PBS,
516 the temporal bone was incubated overnight at room temperature in 0.11M EDTA for
517 decalcification before dissection to expose the auditory epithelium. Samples were then
518 blocked and permeabilized following the same protocol as for earlier stages.
519 The hindbrain (4th ventricle) choroid plexus was dissected at P13 or P15, and fixed in
520 paraformaldehyde (PFA 4%) for 1h at 4°C. After rinsing with PBS, samples were blocked
521 and permeabilized in PBS with 0.5% Triton-X100 and bovine serum albumin (1%) for at
522 least 1h at room temperature before application of the primary antibodies.
523
524 Primary and secondary antibodies were each incubated overnight at 4°C in PBS.
525 Fluorescent-conjugated phalloidin was added with the secondary antibodies. After each
526 antibody incubation, samples were washed 3 times with PBS + 0.05% Triton-X100 before
527 a final post- fixation in PFA 4% for 1h at room temperature. Samples were then mounted
528 flat on a microscopy slide (Denville M1021), either directly under a 18x18mm #1.5
529 coverglass (VWR 48366-045) (cochlea), or using office tape as spacer (choroid plexus).
530 Mowiol was used as mounting medium (Calbiochem/MilliporeSigma 4759041). Mowiol
531 (10% w/v) was prepared in 25%(w/v) glycerol and 0.1M Tris-Cl pH8.5.
532
533 Primary antibodies used were:
534 rabbit anti-MPDZ [34] (gift from Elior Peles, Weizmann Institute of Science; PFA)
535 rabbit anti-CRB3 [51] (gift from Bob Varelas, Boston University; PFA)
536 rabbit anti-TRIOBP/TARA (Proteintech; 16124-1-AP; PFA)
537 rabbit anti-GNAI1/2/3 (Santa Cruz; sc-262; PFA; results in our laboratory indicate that
538 this reagent is not specific for a GNAI paralog and that at least GNAI2 and GNAI3 are
539 co-localized apically in hair cells. We thus use “GNAI” to refer to the signal obtained)
540 rabbit anti-GPSM2 (Sigma; A41537; PFA)
541 mouse anti-aPKC/PRKCZ (Santa Cruz; sc-216; PFA)
542 sheep anti-AFDN/AF-6 (R&D; AF7829; PFA)
543 rat anti-ZO1 (Developmental Studies Hybridoma Bank; R26.4C; TCA or PFA)

544 rabbit anti-MPP5 (Santa Cruz; sc-33831; PFA)
545 rabbit anti-INADL (LifeSpan Biosciences; LS-C410011-50; TCA)
546 rabbit anti-MYO6 (Proteus; 25-6791; PFA)
547 mouse anti-acetylated Tubulin (Santa Cruz; 23950; PFA)
548 Secondary antibodies were raised either in goat or donkey, and coupled to Alexa Fluor
549 (AF) 488, 555 or 647 (ThermoFisher Scientific). We used fluorescent conjugated
550 phalloidins to reveal F-Actin (ThermoFisher Scientific: AF488, A12379, Biotium: CF405,
551 89138-126).
552
553 **Image acquisition and quantification**
554
555 Images were captured using a LSM800 line scanning confocal microscope using the
556 Zen2.3 software, the Airyscan detector in regular confocal mode, and a 63x 1.4 NA oil
557 objective lens (Carl Zeiss AG). When not stated otherwise in the figure legend, all images
558 show a single optical plane. Images were processed using Adobe Photoshop (CC 2020),
559 and the same image treatment was applied across genotypes or conditions in the same
560 experiment. In all experiments, quantifications include three animals of each genotype.
561 All experimental values plotted in the study, as well as animal cohort size and hair cell
562 numbers are detailed in a single Supplementary Data File where each tabulation reports
563 on a single experiment. Results in all 3 OHC rows were pooled because we did not
564 observe a row-specific trend.
565
566 To measure hair cell apical surface area (Figure 1E), z-series stacks were acquired for
567 each sample either at the base or the apex, and a single Z slice was selected based on
568 junctional ZO1 signal. The ZO1-positive outline of the hair cell was traced and the surface
569 area measured using Fiji/ImageJ. To measure immunolabeling signal intensity,
570 microscopy fields were selected where hair cells were mounted as flat as possible so as
571 to avoid artifacts. Z-series stacks were acquired at the cochlear base using the same
572 laser intensity and gain for all samples (mutant and control littermates), and a single Z
573 slice/optical plane was chosen where the signal was the strongest. ZO1 or Afadin/AFDN
574 were used to label the apical hair cell junction, and the base of the stereocilia bundle

575 (phalloidin) was used to distinguish the bare zone (lateral) and the medial sides of the
576 apical membrane. Fiji/ImageJ was used to measure the Mean gray value in a region of
577 interest (ROI) as defined below. For each image, background signal was sampled and
578 averaged, then subtracted to all hair cell quantifications on the same image.
579
580 To measure GNAI signal intensity in *Mpdz* mutants (Figure 2D), the lateral (bare zone)
581 and medial compartments were divided in 3 ROIs of equal width (a, b, c; see Figure 2D),
582 and the Mean gray value of each region was measured. To obtain the Mean gray value
583 of the entire bare zone and medial compartments (Figure 2B), values in the 3 ROIs were
584 averaged. To measure aPKC (Figure 3B) and MPP5 (Figure 4F) signals in *Mpdz* mutants,
585 a fixed ROI was positioned so as to cover about 50% of the apical compartments
586 considered (bare zone, medial apex, hair bundle). To measure MPP5 intensity at
587 junctions (Figure 4G), a rectangular ROI of 0.85 μm^2 (1.67 x 0.51µm) was positioned at
588 the medial hair cell junction. To measure MPDZ intensity in *Gpsm2* mutants (Figure 5B-
589 C), a circular ROI of 1.054 μm^2 was positioned at the lateral (bare zone) and medial apical
590 compartments.
591
592 **Scanning Electron Microscopy (SEM)**
593
594 Temporal bones were isolated from the skull, a hole was punctured at the cochlear apex,
595 and samples were immersion-fixed for at least one overnight at 4°C in 2.5%
596 glutaraldehyde + 4% paraformaldehyde (Electron Microscopy Science) in a 1mM $MgCl_2$,
597 0.1M Sodium Cacodylate, 20mM $CaCl_2$ buffer. After rinses in PBS, samples were
598 decalcified overnight with 0.11M EDTA and the auditory epithelium was dissected in 3
599 pieces (cochlear base, mid, apex). Dissected samples were progressively dehydrated in
600 an ethanol series (30-50-70-80-90-100%, for at least 20 minutes each). Chemical sample
601 drying was done with hexamethyldisilazane (HMDS; Electron Microscopy Science 50-
602 243-18). Dry samples were then mounted on aluminum stubs using double-sided carbon
603 tape, and sputter-coated with gold-palladium before imaging on a Hitachi 3000N VP
604 electron microscope. Images were taken at 20kV and with a 5k magnification.
605

606 **Auditory Brainstem Response (ABR) tests**

607

608 Mice were anesthetized by intraperitoneal injection of a mix of ketamine and xylazine (10
609 mg and 0.1 mg per 10g of body weight, respectively) and body temperature was
610 maintained at 37°C using a heating pad (FHC). All tests were conducted in a sound-
611 attenuating chamber. ABR testing was done using the RZ6 Multi-I/O Processor System
612 coupled to the RA4PA 4-channel Medusa Amplifier (Tucker-Davis Technology). Tone
613 bursts at 8, 16, 32 and 40 kHz were generated with the TDT system, and sub-dermal
614 needles were used as electrodes, with the active electrode inserted at the cranial vertex,
615 the reference electrode under the left ear, and the ground electrode at the right thigh.
616 Auditory thresholds were obtained for each stimulus by reducing the Sound Pressure
617 Level (SPL) by 5 dB steps between 90 and 20 dB to determine at which SPL an ABR
618 could be recognized. *Mpdz*$^{DEL/DEL}$ mutants and *Mpdz*$^{DEL/+}$ control littermates were tested
619 between age P21 and P24. Both sexes were tested (see detailed Supplementary Data
620 File), and because sex had no influence on thresholds, sexes were pooled in Figure 6E.

621

622 **Statistical Analysis**

623

624 Data were plotted in Prism 8(GraphPad). All values were plotted individually, and the
625 distribution was framed with 25-75% whisker boxes where exterior lines show the
626 minimum and maximum, the middle line representing the median, and + is used for the
627 mean. A potential difference in data distribution between genotypes was tested for
628 significance using the Mann-Whitney U test (non-parametric unpaired t-test), except in
629 the following cases: i) GNAI signal intensity by sub-region at the bare zone (Figure 2D),
630 where we used a Wilcoxon signed-rank paired test to compare the 3 different sub-regions
631 (a, b, c). ii) ABR thresholds (Figure 6D), where we used the 2-way ANOVA test coupled
632 with a Sidak's multiple comparison. Exact p-values are indicated in the figure legends,
633 and p-values are summarized on graphical plots with the following "star": system:
634 $p<0.0001$ = ****, $0.0001<p<0.001$ = ***, $0.001<p<0.01$ = **, $0.01<p<0.05$ = *, $p>0.05$ = not
635 significant (ns). When not quantified, all immunolabeling experiments included at least 3

636 mutant samples in two litters, and a similar number of littermate control animals. In that
637 case, figure panels show a representative outcome observed in all mutant samples.

638

639

640

641

642

643 REFERENCES

644

645 1. Petit, C. and G.P. Richardson, *Linking genes underlying deafness to hair-bundle*
646 *development and function.* Nat Neurosci, 2009. **12**(6): p. 703-10.
647 2. McGrath, J., P. Roy, and B.J. Perrin, *Stereocilia morphogenesis and maintenance*
648 *through regulation of actin stability.* Semin Cell Dev Biol, 2017. **65**: p. 88-95.
649 3. Velez-Ortega, A.C. and G.I. Frolenkov, *Building and repairing the stereocilia*
650 *cytoskeleton in mammalian auditory hair cells.* Hear Res, 2019. **376**: p. 47-57.
651 4. Barr-Gillespie, P.G., *Assembly of hair bundles, an amazing problem for cell biology.* Mol
652 Biol Cell, 2015. **26**(15): p. 2727-32.
653 5. Beer-Hammer, S., et al., *Galphai Proteins are Indispensable for Hearing.* Cell Physiol
654 Biochem, 2018. **47**(4): p. 1509-1532.
655 6. Ezan, J., et al., *Primary cilium migration depends on G-protein signalling control of*
656 *subapical cytoskeleton.* Nat Cell Biol, 2013. **15**(9): p. 1107-15.
657 7. Mauriac, S.A., et al., *Defective Gpsm2/Galphai3 signalling disrupts stereocilia*
658 *development and growth cone actin dynamics in Chudley-McCullough syndrome.* Nat
659 Commun, 2017. **8**: p. 14907.
660 8. Tarchini, B., C. Jolicoeur, and M. Cayouette, *A molecular blueprint at the apical surface*
661 *establishes planar asymmetry in cochlear hair cells.* Dev Cell, 2013. **27**(1): p. 88-102.
662 9. Tarchini, B., et al., *A link between planar polarity and staircase-like bundle architecture*
663 *in hair cells.* Development, 2016. **143**(21): p. 3926-3932.
664 10. Tadenev, A.L.D., et al., *GPSM2-GNAI Specifies the Tallest Stereocilia and Defines Hair*
665 *Bundle Row Identity.* Curr Biol, 2019. **29**(6): p. 921-934 e4.
666 11. Bhonker, Y., et al., *The GPSM2/LGN GoLoco motifs are essential for hearing.* Mamm
667 Genome, 2016. **27**(1-2): p. 29-46.
668 12. Doherty, D., et al., *GPSM2 mutations cause the brain malformations and hearing loss in*
669 *Chudley-McCullough syndrome.* Am J Hum Genet, 2012. **90**(6): p. 1088-93.
670 13. Walsh, T., et al., *Whole exome sequencing and homozygosity mapping identify mutation*
671 *in the cell polarity protein GPSM2 as the cause of nonsyndromic hearing loss DFNB82.*
672 Am J Hum Genet, 2010. **87**(1): p. 90-4.
673 14. Tarchini, B. and X. Lu, *New insights into regulation and function of planar polarity in the*
674 *inner ear.* Neurosci Lett, 2019. **709**: p. 134373.
675 15. Deans, M.R., *A balance of form and function: planar polarity and development of the*
676 *vestibular maculae.* Semin Cell Dev Biol, 2013. **24**(5): p. 490-8.
677 16. Landin Malt, A., et al., *Wnts regulate planar cell polarity via heterotrimeric G protein and*
678 *PI3K signaling.* J Cell Biol, 2020. **219**(10).
679 17. Najarro, E.H., et al., *Dual regulation of planar polarization by secreted Wnts and Vangl2*
680 *in the developing mouse cochlea.* Development, 2020. **147**(19).
681 18. Siletti, K., B. Tarchini, and A.J. Hudspeth, *Daple coordinates organ-wide and cell-*
682 *intrinsic polarity to pattern inner-ear hair bundles.* Proc Natl Acad Sci U S A, 2017.
683 **114**(52): p. E11170-E11179.
684 19. Landin Malt, A., et al., *Par3 is essential for the establishment of planar cell polarity of*
685 *inner ear hair cells.* Proc Natl Acad Sci U S A, 2019. **116**(11): p. 4999-5008.
686 20. Ullmer, C., et al., *Cloning and characterization of MUPP1, a novel PDZ domain protein.*
687 FEBS letters, 1998. **424**(1-2).
688 21. Simpson, E., R. Suffolk, and I. Jackson, *Identification, sequence, and mapping of the*
689 *mouse multiple PDZ domain protein gene, Mpdz.* Genomics, 1999. **59**(1).

690 22. Krapivinsky, G., et al., *SynGAP-MUPP1-CaMKII synaptic complexes regulate p38 MAP*
691 *kinase activity and NMDA receptor-dependent synaptic AMPA receptor potentiation.*
692 Neuron, 2004. **43**(4).
693 23. Tetzlaff, F., et al., *MPDZ promotes DLL4-induced Notch signaling during angiogenesis.*
694 Elife, 2018. **7**.
695 24. Lemmers, C., et al., *hINADl/PATJ, a homolog of discs lost, interacts with crumbs and*
696 *localizes to tight junctions in human epithelial cells.* J Biol Chem, 2002. **277**(28): p.
697 25408-15.
698 25. Makarova, O., et al., *Mammalian Crumbs3 is a small transmembrane protein linked to*
699 *protein associated with Lin-7 (Pals1).* Gene, 2003. **302**(1-2): p. 21-9.
700 26. Roh, M.H., et al., *The Crumbs3-Pals1 complex participates in the establishment of*
701 *polarity in mammalian epithelial cells.* J Cell Sci, 2003. **116**(Pt 14): p. 2895-906.
702 27. Roh, M.H., et al., *The Maguk protein, Pals1, functions as an adapter, linking mammalian*
703 *homologues of Crumbs and Discs Lost.* J Cell Biol, 2002. **157**(1): p. 161-72.
704 28. Tepass, U., *The apical polarity protein network in Drosophila epithelial cells: regulation*
705 *of polarity, junctions, morphogenesis, cell growth, and survival.* Annu Rev Cell Dev Biol,
706 2012. **28**: p. 655-85.
707 29. Assémat, E., et al., *Polarity complex proteins.* Biochim Biophys Acta, 2008. **1778**(3): p.
708 614-30.
709 30. Hurd, T.W., et al., *Direct interaction of two polarity complexes implicated in epithelial*
710 *tight junction assembly.* Nat Cell Biol, 2003. **5**(2): p. 137-42.
711 31. Shin, K., S. Straight, and B. Margolis, *PATJ regulates tight junction formation and*
712 *polarity in mammalian epithelial cells.* J Cell Biol, 2005. **168**(5): p. 705-11.
713 32. Charrier, L.E., E. Loie, and P. Laprise, *Mouse Crumbs3 sustains epithelial tissue*
714 *morphogenesis in vivo.* Sci Rep, 2015. **5**: p. 17699.
715 33. Whiteman, E.L., et al., *Crumbs3 is essential for proper epithelial development and*
716 *viability.* Mol Cell Biol, 2014. **34**(1): p. 43-56.
717 34. Poliak, S., et al., *Distinct claudins and associated PDZ proteins form different autotypic*
718 *tight junctions in myelinating Schwann cells.* J Cell Biol, 2002. **159**(2): p. 361-72.
719 35. Hamazaki, Y., et al., *Multi-PDZ domain protein 1 (MUPP1) is concentrated at tight*
720 *junctions through its possible interaction with claudin-1 and junctional adhesion*
721 *molecule.* J Biol Chem, 2002. **277**(1): p. 455-61.
722 36. Lanaspa, M.A., et al., *Hypertonic stress increases claudin-4 expression and tight*
723 *junction integrity in association with MUPP1 in IMCD3 cells.* Proc Natl Acad Sci U S A,
724 2008. **105**(41): p. 15797-802.
725 37. Adachi, M., et al., *Similar and distinct properties of MUPP1 and Patj, two homologous*
726 *PDZ domain-containing tight-junction proteins.* Mol Cell Biol, 2009. **29**(9): p. 2372-89.
727 38. Marivin, A., et al., *GPCR-independent activation of G proteins promotes apical cell*
728 *constriction in vivo.* J Cell Biol, 2019. **218**(5): p. 1743-1763.
729 39. Marivin, A. and M. Garcia-Marcos, *DAPLE and MPDZ bind to each other and cooperate*
730 *to promote apical cell constriction.* Mol Biol Cell, 2019. **30**(16): p. 1900-1910.
731 40. Saugier-Veber, P., et al., *Hydrocephalus due to multiple ependymal malformations is*
732 *caused by mutations in the MPDZ gene.* Acta Neuropathol Commun, 2017. **5**(1): p. 36.
733 41. Feldner, A., et al., *Loss of Mpdz impairs ependymal cell integrity leading to perinatal-*
734 *onset hydrocephalus in mice.* EMBO Mol Med, 2017. **9**(7): p. 890-905.
735 42. Yang, J., et al., *Murine MPDZ-linked hydrocephalus is caused by hyperpermeability of*
736 *the choroid plexus.* EMBO Mol Med, 2019. **11**(1).
737 43. Al-Dosari, M., et al., *Mutation in MPDZ causes severe congenital hydrocephalus.* Journal
738 of medical genetics, 2013. **50**(1).

739 44. Al-Jezawi, N.K., et al., *Compound heterozygous variants in the multiple PDZ domain*
740 *protein (MPDZ) cause a case of mild non-progressive communicating hydrocephalus.*
741 BMC Medical Genetics, 2018. **19**(1): p. 1-11.
742 45. Shaheen, R., et al., *The genetic landscape of familial congenital hydrocephalus.* Annals
743 of neurology, 2017. **81**(6).
744 46. Milner, L.C., et al., *Novel MPDZ/MUPP1 transgenic and knockdown models confirm*
745 *Mpdz's role in ethanol withdrawal and support its role in voluntary ethanol consumption.*
746 Addict Biol, 2015. **20**(1): p. 143-7.
747 47. Katsuno, T., et al., *TRIOBP-5 sculpts stereocilia rootlets and stiffens supporting cells*
748 *enabling hearing.* JCI Insight, 2019. **4**(12).
749 48. Etournay, R., et al., *Cochlear outer hair cells undergo an apical circumference*
750 *remodeling constrained by the hair bundle shape.* Development, 2010. **137**(8): p. 1373-
751 83.
752 49. McKenzie, E., A. Krupin, and M.W. Kelley, *Cellular growth and rearrangement during the*
753 *development of the mammalian organ of Corti.* Dev Dyn, 2004. **229**(4): p. 802-12.
754 50. Straight, S.W., et al., *Loss of PALS1 expression leads to tight junction and polarity*
755 *defects.* Mol Biol Cell, 2004. **15**(4): p. 1981-90.
756 51. Szymaniak, A.D., et al., *Crumbs3-Mediated Polarity Directs Airway Epithelial Cell Fate*
757 *through the Hippo Pathway Effector Yap.* Dev Cell, 2015. **34**(3): p. 283-96.
758 52. Assemat, E., et al., *The multi-PDZ domain protein-1 (MUPP-1) expression regulates*
759 *cellular levels of the PALS-1/PATJ polarity complex.* Exp Cell Res, 2013. **319**(17): p.
760 2514-25.
761 53. Gao, Y., et al., *Polarity protein Crumbs homolog-3 (CRB3) regulates ectoplasmic*
762 *specialization dynamics through its action on F-actin organization in Sertoli cells.*
763 Scientific reports, 2016. **6**.
764 54. Jin, Y., et al., *Deletion of Brg1 causes abnormal hair cell planer polarity, hair cell*
765 *anchorage, and scar formation in mouse cochlea.* Scientific Reports, 2016. **6**(1): p. 1-14.
766 55. Freeman, S., et al., *Proteostasis is essential during cochlear development for neuron*
767 *survival and hair cell polarity.* EMBO Rep, 2019. **20**(9): p. e47097.
768 56. Tapanes-Castillo, A., et al., *A modifier locus on chromosome 5 contributes to L1 cell*
769 *adhesion molecule X-linked hydrocephalus in mice.* Neurogenetics, 2010. **11**(1).
770 57. Tan, B., et al., *The Mammalian Crumbs Complex Defines a Distinct Polarity Domain*
771 *Apical of Epithelial Tight Junctions.* Curr Biol, 2020. **30**(14): p. 2791-2804 e6.
772 58. Takagishi, M., et al., *Daple Coordinates Planar Polarized Microtubule Dynamics in*
773 *Ependymal Cells and Contributes to Hydrocephalus.* Cell Rep, 2017. **20**(4): p. 960-972.
774 59. Ekici, A.B., et al., *Disturbed Wnt Signalling due to a Mutation in CCDC88C Causes an*
775 *Autosomal Recessive Non-Syndromic Hydrocephalus with Medial Diverticulum.* Mol
776 Syndromol, 2010. **1**(3): p. 99-112.
777 60. Drielsma, A., et al., *Two novel CCDC88C mutations confirm the role of DAPLE in*
778 *autosomal recessive congenital hydrocephalus.* J Med Genet, 2012. **49**(11): p. 708-12.

779

780

781

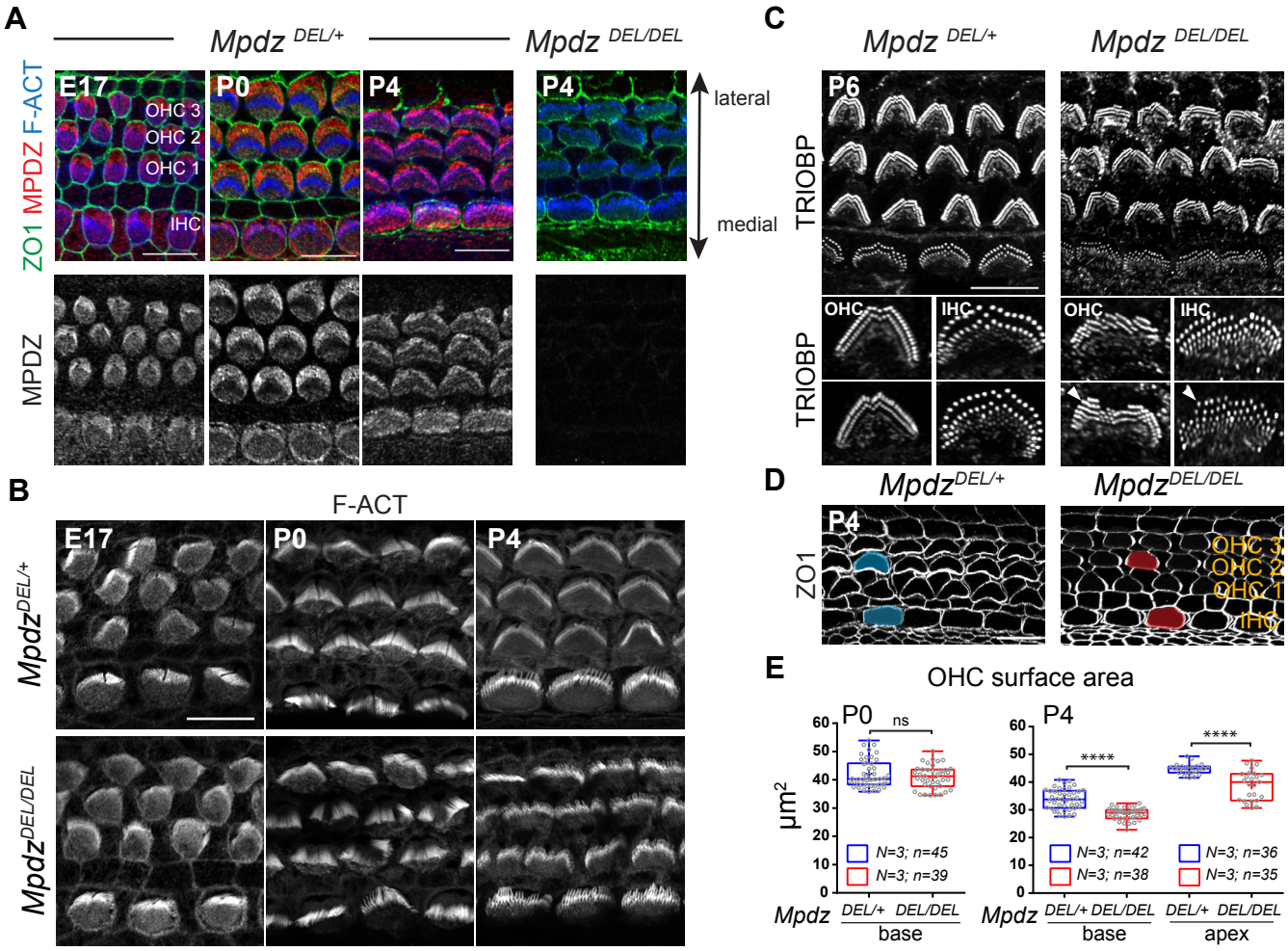
A
Mpdz DEL/+
Mpdz DEL/DEL
ZO1 MPDZ F-ACT
E17
P0
P4
P4
OHC 3
OHC 2
OHC 1
IHC
lateral
medial
MPDZ
B
F-ACT
E17
P0
P4
MpdzDEL/+
MpdzDEL/DEL
C
Mpdz DEL/+
Mpdz DEL/DEL
P6
TRIOBP
TRIOBP
OHC
IHC
OHC
IHC
D
MpdzDEL/+
MpdzDEL/DEL
P4
ZO1
OHC 3
OHC 2
OHC 1
IHC
E
OHC surface area
P0
ns
P4
****
****
µm2
N=3; n=45
N=3; n=39
N=3; n=42
N=3; n=38
N=3; n=36
N=3; n=35
Mpdz DEL/+ DEL/DEL
base
Mpdz DEL/+ DEL/DEL
base
DEL/+ DEL/DEL
apex

Figure 1

Figure 1. MPDZ occupies the hair cell apical membrane and is required for normal junction circumferences and stereocilia distribution in neonates. A) Flat mount views of the mouse auditory epithelium immunolabeled with MPDZ (red), ZO1 (green, apical junctions) and phalloidin (blue, F-actin) at E17, P0 and P4 (cochlear base). MPDZ signal is entirely lost in *Mpdz* mutants (*Mpdz*$^{DEL/DEL}$). **B)** Phalloidin (F-actin) labeling of the hair bundle level (cochlear base; maximal projection). In absence of MPDZ, OHC and IHC hair bundles are misshapen from P0. **C)** TRIOBP labeling of the stereocilia rootlets at P6 (maximal projection). Stereocilia are misaligned and form interrupted or supernumerary rows in *Mpdz* mutants. **D)** ZO1 labeling of the apical junctions (cochlear base) at P4. In absence of MPDZ, the HC circumference is abnormally rounded, and the apical surface appears reduced. **E)** Apical OHC surface area at P0 and P4 based on ZO1 labeling. Here and in the following figures, graphical representations show a boxplot with 25-75% percentiles where external bars show the minimum and maximum, the internal bar shows the median and the cross shows the mean. All points are also shown. N = number of animals, n = total number of OHCs (Mann-Whitney U test; P0: $p=0.4417$ ^{ns}; P4 base: $p<0.0001$ ****; P4 apex: $p<0.0001$****; ns, not significant). Scale bars are 10µm.

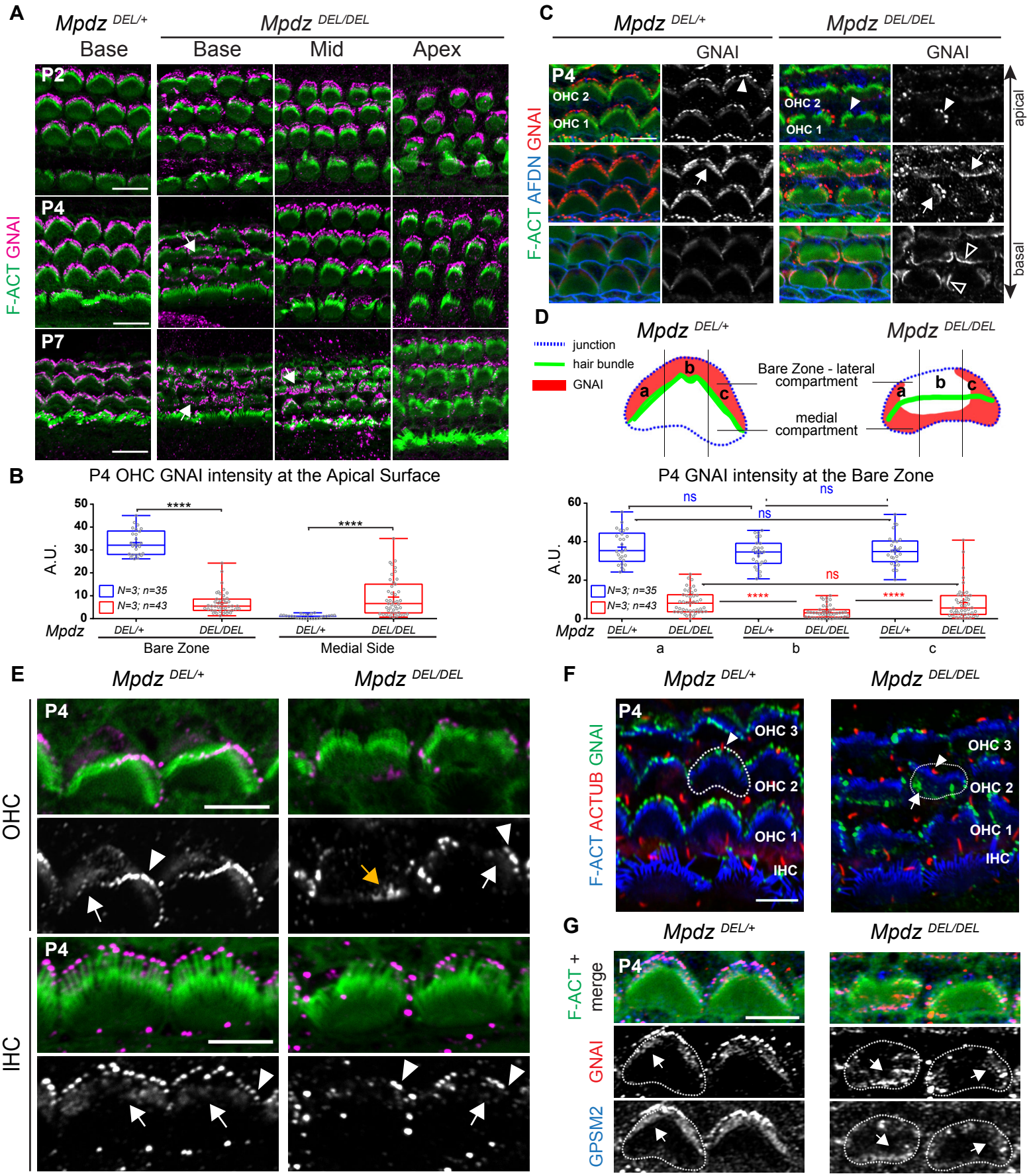
A
Mpdz DEL/+
Mpdz DEL/DEL
Base
Base
Mid
Apex
P2
P4
P7
F-ACT GNAI
C
Mpdz DEL/+
Mpdz DEL/DEL
GNAI
GNAI
P4
OHC 2
OHC 1
F-ACT AFDN GNAI
apical
basal
D
Mpdz DEL/+
Mpdz DEL/DEL
junction
hair bundle
GNAI
a
b
c
Bare Zone - lateral compartment
medial compartment
B
P4 OHC GNAI intensity at the Apical Surface
A.U.
****
****
N=3; n=35
N=3; n=43
Mpdz
DEL/+
DEL/DEL
DEL/+
DEL/DEL
Bare Zone
Medial Side
P4 GNAI intensity at the Bare Zone
ns
ns
ns
ns
****
****
a
b
c
E
Mpdz DEL/+
Mpdz DEL/DEL
P4
OHC
IHC
F
Mpdz DEL/+
Mpdz DEL/DEL
P4
OHC 3
OHC 2
OHC 1
IHC
F-ACT ACTUB GNAI
G
Mpdz DEL/+
Mpdz DEL/DEL
P4
F-ACT + merge
GNAI
GPSM2

Figure 2

Figure 2. Apical enrichment of GNAI and GPSM2 is progressively reduced and delocalized in absence of MPDZ. A) GNAI immunolabeling (magenta) at different postnatal stages and positions along the cochlea (maximal projection). In *Mpdz* mutants, GNAI enrichment at the lateral bare zone and in neighboring stereocilia is compromised at the cochlear base at P4 (arrows), and this defect extends to the cochlear mid by P7. **B)** GNAI enrichment at the lateral (bare zone) and medial apical surface in P4 OHCs. N = number of animals, n = total number of OHCs **(**Mann-Whitney U test; Bare zone and medial side: $p<0.0001$ ****). **C)** GNAI labeling at P4 at 3 different apico-basal Z levels of the same confocal stack (OHC1-2 field at the cochlear base). F-actin labels stereocilia and Afadin (AFDN) labels the apical junctions. In *Mpdz* mutants, GNAI enrichment is generally reduced, and often delocalized medially at the flat HC apex (arrows) and partially lost in the stereocilia (solid arrowheads). GNAI is also ectopically detected at medial apical junctions below the flat apex (hollow arrowheads). **D)** GNAI enrichment across the bare zone in P4 OHCs. The schematic depicts GNAI enrichment compared to the HC junction and the hair bundle in control and *Mpdz* mutant. The OHCs apical surface was divided in 3 regions of equal width (a, b, c) and GNAI signal was measured by region. N = number of animals, n = number of OHCs**.** Wilcoxon signed-rank test ($Mpdz^{DEL/+}$*:* a vs b $p= 0.1307$ ^{ns}; b vs c $p= 0.3707$ ^{ns}; a vs c $p= 0.9525$ ^{ns}; $Mpdz^{DEL/DEL}$*:* a vs b and b vs c $p< 0.0001$ ****; a vs c $p= 0.7880$ ^{ns}). **E)** GNAI enrichment at higher magnification in two representative P4 OHCs and IHCs (cochlear base; maximal projection). Note how in *Mpdz* mutant HCs, GNAI signal is reduced, particularly at the flat HC apex. In OHCs, GNAI is only retained in a subset of peripheral stereocilia (arrowheads) adjacent to where GNAI is retained at the peripheral region of the bare zone (arrows). Alternatively, GNAI is delocalized medially at the HC flat surface (orange arrows) and missing in the hair bundle entirely (orange arrowheads). **F)** Co-immunolabeling of GNAI (green) and acetylated tubulin (ACTUB, red) to reveal the kinocilium at P4 (cochlear base; maximal projection). A single OHC2 is outlined in each panel. As in control HCs, the kinocilium (arrowheads) is localized lateral to the hair bundle in *Mpdz* mutant OHCs, even when GNAI is delocalized medially (arrows). **G)** GNAI-GPSM2 co-labeling in P4 OHCs (cochlear base). Delocalized GNAI and GPSM2 (arrows) still co-localize in *Mpdz* mutants. Scale bars are 10µm (A), 5µm (C and E-G).

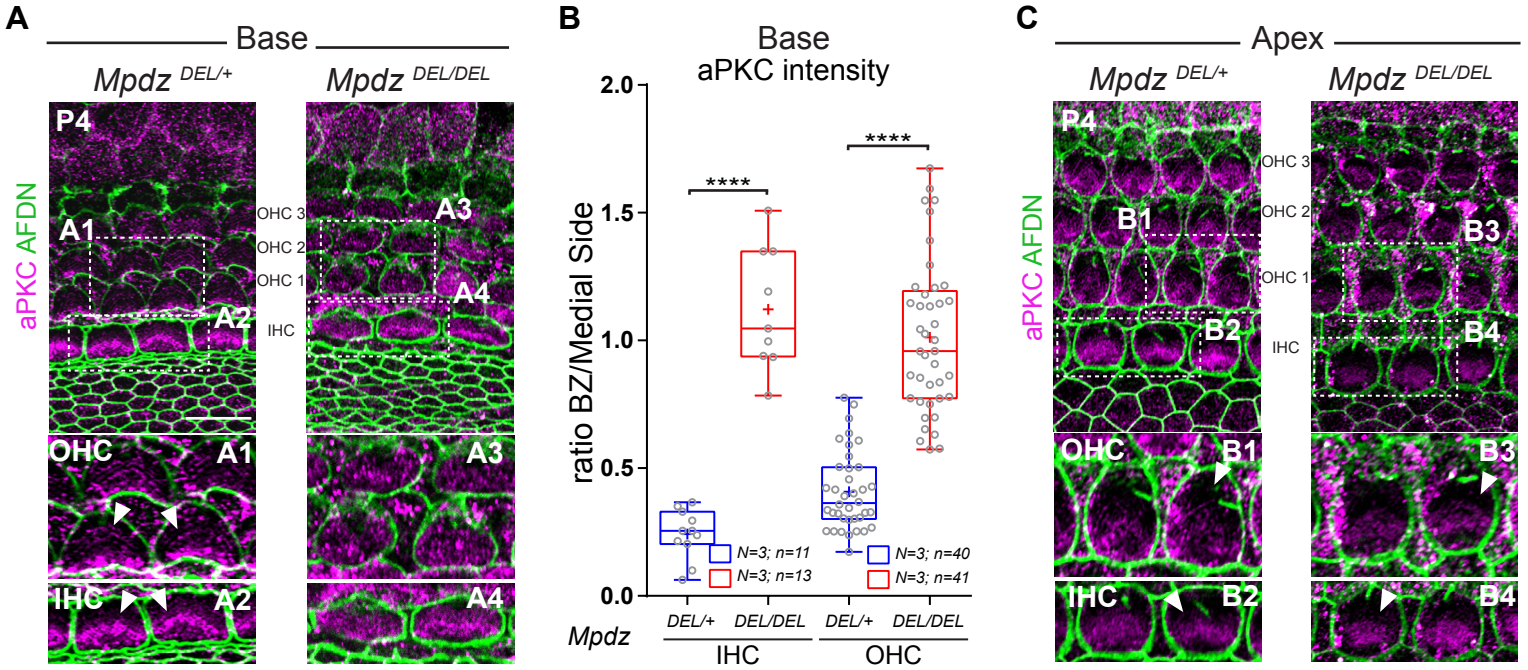
A
Base
Mpdz DEL/+
Mpdz DEL/DEL
P4
A1
A2
A3
A4
OHC 3
OHC 2
OHC 1
IHC
OHC
aPKC AFDN
B
Base
aPKC intensity
ratio BZ/Medial Side
2.0
1.5
1.0
0.5
0.0
****
****
N=3; n=11
N=3; n=13
N=3; n=40
N=3; n=41
DEL/+
DEL/DEL
DEL/+
DEL/DEL
Mpdz
IHC
OHC
C
Apex
Mpdz DEL/+
Mpdz DEL/DEL
P4
B1
B2
B3
B4
OHC 3
OHC 2
OHC 1
IHC
OHC
aPKC AFDN

Figure 3

Figure 3. aPKC medial restriction at the apical membrane is lost in absence of MPDZ. aPKC labeling (magenta) at P4 at the cochlear base (A) and apex (C). Apical junctions are labeled with Afadin (AFDN; green). **A)** The lateral bare zone devoid of aPKC signal in controls (arrowheads) shows ectopic aPKC signal in *Mpdz* mutants in both OHCs and IHCs. **B)** aPKC enrichment at the HC apical surface at the cochlear base. The ratio between signal intensity at the bare zone (BZ) and at the medial side is plotted (see Supplementary Data File for values by compartments). N = number of animals, n = number of HCs (Mann-Whitney U test; OHC and IHC: $p<0.0001$ ****). **C)** At the cochlear apex, aPKC is normally excluded from the bare zone in *Mpdz* mutants. The boxed regions (A1-A4; B1-B4) are magnified in the bottom panels. Scale bars are 10µm.

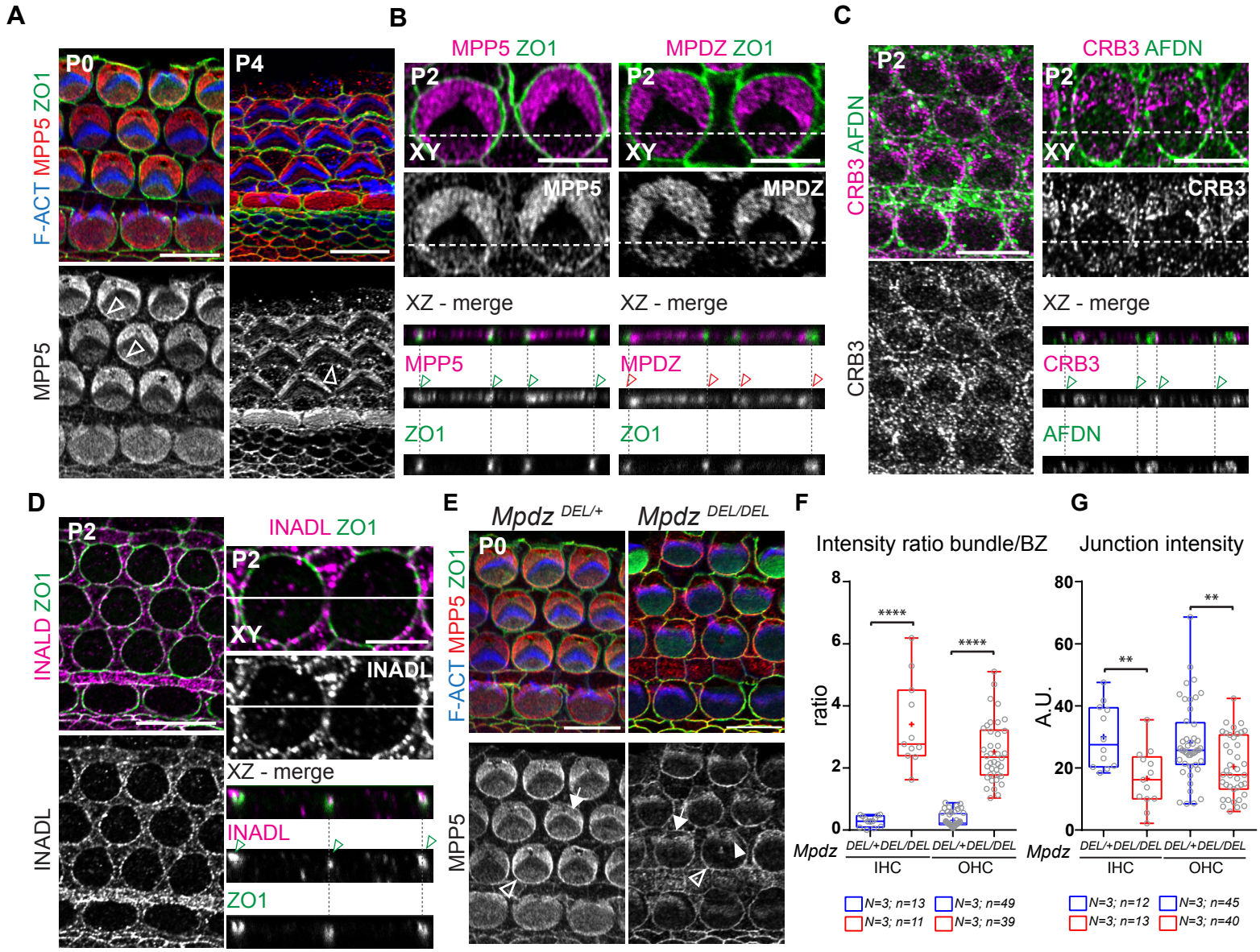
A
F-ACT MPP5 ZO1
P0
P4
MPP5
B
MPP5 ZO1
MPDZ ZO1
P2
XY
MPP5
MPDZ
XZ - merge
MPP5
MPDZ
ZO1
C
CRB3 AFDN
CRB3
D
INALD ZO1
INADL
INADL ZO1
XZ - merge
E
Mpdz DEL/+
Mpdz DEL/DEL
F-ACT MPP5 ZO1
MPP5
F
Intensity ratio bundle/BZ
ratio
Mpdz
DEL/+ DEL/DEL
IHC
OHC
N=3; n=13
N=3; n=11
N=3; n=49
N=3; n=39
G
Junction intensity
A.U.
N=3; n=12
N=3; n=13
N=3; n=45
N=3; n=40

Figure 4

Figure 4. MPDZ coincides with MPP5/PALS1 and CRB3 and is required for their correct distribution at the hair cell apical membrane. A-D) Immunolabeling in flat (XY) and projection (XZ) views of the auditory epithelium between P0 and P4. **A)** MPP5 immunolabeling reveals a similar protein distribution to MPDZ (Fig. 1A). **B)** Projections also show MPP5 co-enrichment with ZO1 at the HC-support cell junctions (green arrowheads). MPP5 is enriched on both the HC and support cell membrane (see Supp. Fig. 1A). In contrast, MPDZ is not co-detected with ZO1 at apical junctions (red arrowheads). **C)** CRB3 distribution is similar to MPP5 (A-B), encompassing both the apical membrane and the apical junctions (green arrowheads). Afadin/AFDN was used to visualize apical junctions as ZO1 signal was compromised by the antigen retrieval procedure. **D)** INADL/PATJ is only detected at apical junctions with ZO1 (green arrowheads), and not at the apical surface. INADL appears to be enriched only on the support cell membrane (see Supp. Fig. 1B). **E)** MPP5 labeling in P0 *Mpdz* mutant. In absence of MPDZ, MPP5 is lost at the bare zone (arrow) and ectopically found in the hair bundle (solid arrowhead). MPP5 is retained at apical junctions (hollow arrowheads). **F-G)** Apical MPP5 enrichment in P0 HCs at the cochlear base. The ratio between the MPP5 signals at the hair bundle and bare zone (F) and the MPP5 signal at the medial apical junction (G) are plotted. N = number of animals, n = number of HCs (Mann-Whitney U test; (F) IHC and OHC: $p<0.0001$ ****; (G) IHC: $p=0.00086$ **, OHC $p=0.0079$ **). Cochlear base (A, C left, D left, E), cochlear mid (B, C right, D right). Scale bars are 10µm.

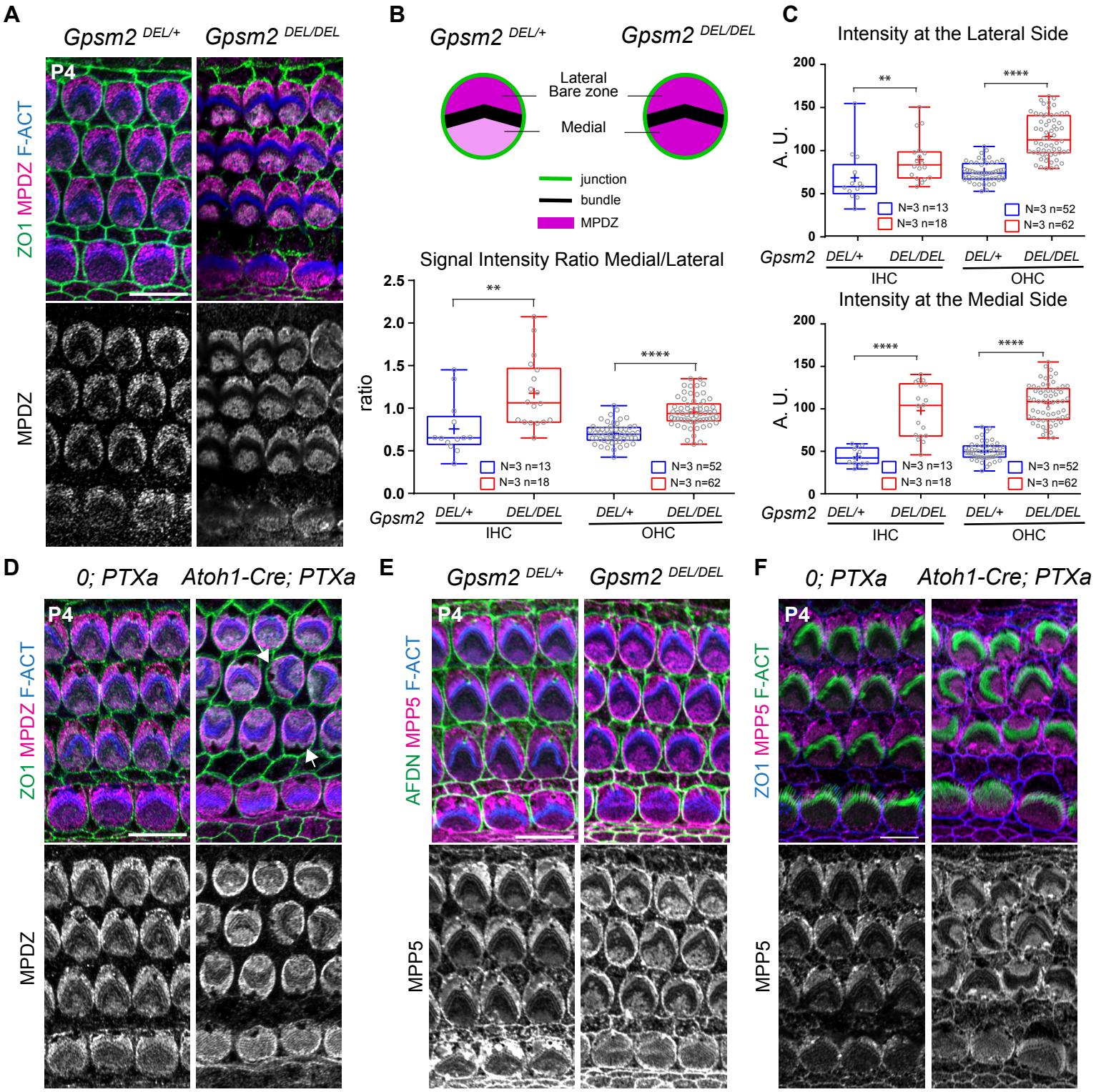
A
Gpsm2 DEL/+
Gpsm2 DEL/DEL
P4
ZO1 MPDZ F-ACT
MPDZ
B
Gpsm2 DEL/+
Gpsm2 DEL/DEL
Lateral
Bare zone
Medial
junction
bundle
MPDZ
Signal Intensity Ratio Medial/Lateral
ratio
2.5
2.0
1.5
1.0
0.5
0.0
**
****
N=3 n=13
N=3 n=18
N=3 n=52
N=3 n=62
Gpsm2
DEL/+
DEL/DEL
IHC
OHC
C
Intensity at the Lateral Side
A. U.
200
150
100
50
0
**
****
N=3 n=13
N=3 n=18
N=3 n=52
N=3 n=62
Gpsm2
DEL/+
DEL/DEL
IHC
OHC
Intensity at the Medial Side
A. U.
200
150
100
50
0
****
****
N=3 n=13
N=3 n=18
N=3 n=52
N=3 n=62
Gpsm2
DEL/+
DEL/DEL
IHC
OHC
D
0; PTXa
Atoh1-Cre; PTXa
P4
ZO1 MPDZ F-ACT
MPDZ
E
Gpsm2 DEL/+
Gpsm2 DEL/DEL
P4
AFDN MPP5 F-ACT
MPP5
F
0; PTXa
Atoh1-Cre; PTXa
P4
ZO1 MPP5 F-ACT
MPP5

Figure 5

Figure 5. GNAI-GPSM2 promotes planar polarization of MPDZ and MPP5 at the apical membrane. A) MPDZ labeling (magenta) in *Gpsm*$^{DEL/DEL}$ HCs at P4 (cochlear apex). MPDZ lacks higher enrichment at the lateral bare zone in absence of GPSM2. **B-C)** MPDZ enrichment in *Gpsm2* mutant HCs at P4 (cochlear apex). The ratio between the medial and lateral (bare zone) MPDZ signals (B), and the individual signals at the bare zone (C, top) and medial apex (C, bottom) are plotted. Note how MPDZ signals increase in both compartments in *Gpsm2* mutants, but more strongly at the medial apex. N = number of animals, n = number of HCs (Mann-Whitney U test; (B) IHC: p=0.0014 ***, OHC: p<0.0001****; (C) Lateral IHC: p=0.0064 **, OHC: p<0.0001 ****; Medial IHC and OHC: p<0.0001 ****). **D)** MPDZ labeling (magenta) in Pertussis toxin (PTXa)-expressing HCs at P4 (cochlear apex). MPDZ lacks higher enrichment at the lateral bare zone when GNAI is inactivated by PTXa. GNAI inactivation provokes graded OHCs misorientation so that the bare zone region (arrows) is not consistently lateral in PTXa OHCs. **E-F)** MPP5 labeling (magenta) in *Gpsm*$^{DEL/DEL}$ (E) and PTXa (F) HCs at P4 (cochlear apex). Like MPDZ (A-D), MPP5 is more uniformly enriched across the apical membrane when GPSM2 or GNAI is inactivated. In (E), Afadin (AFDN) is used instead of ZO1 to label the apical junctions. Scale bars are 10μm.

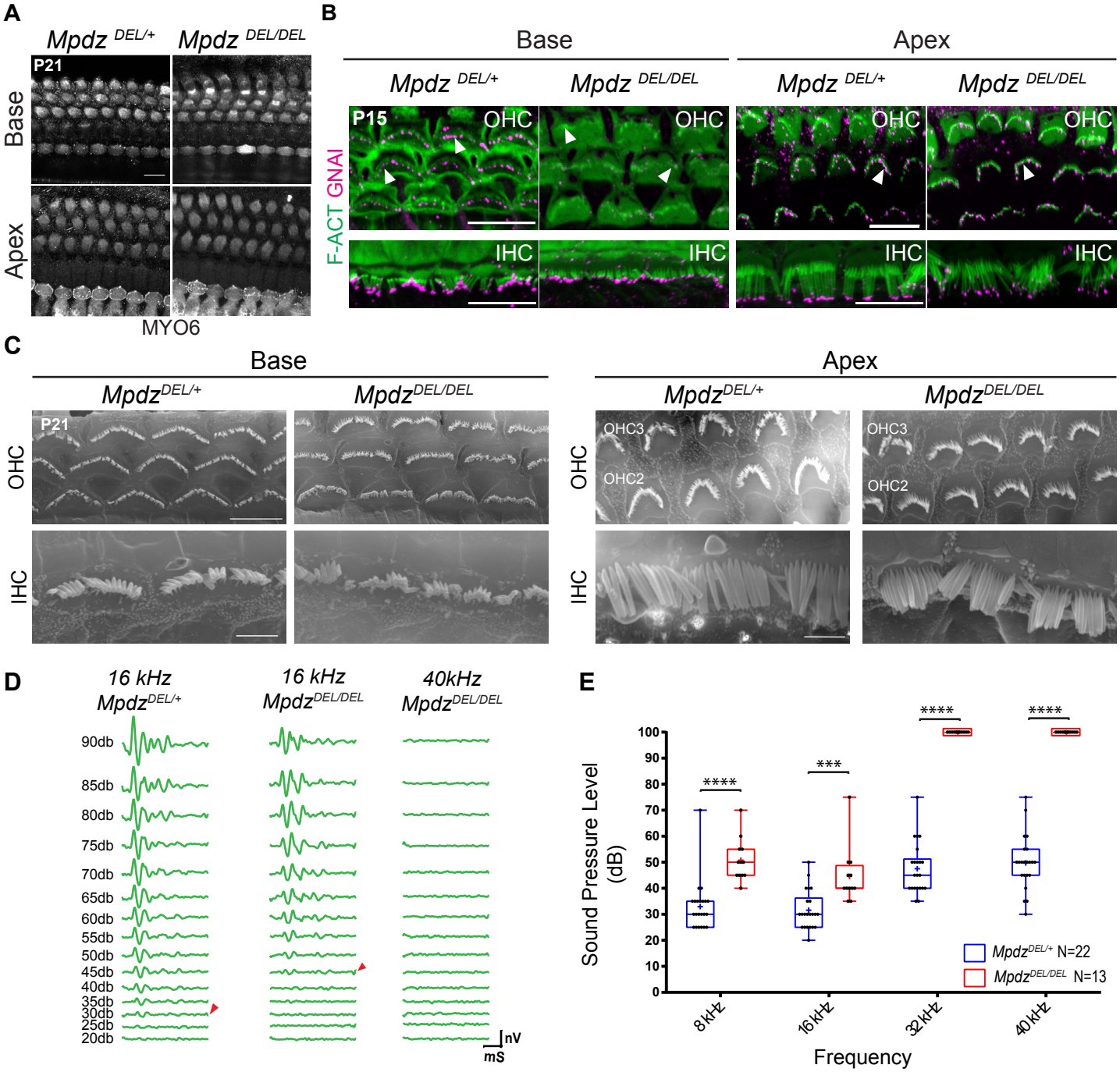
A
Mpdz DEL/+
Mpdz DEL/DEL
P21
Base
Apex
MYO6
B
Base
Apex
Mpdz DEL/+
Mpdz DEL/DEL
P15
OHC
IHC
F-ACT GNAI
C
Base
Apex
Mpdz DEL/+
Mpdz DEL/DEL
P21
OHC
IHC
OHC3
OHC2
D
16 kHz
Mpdz DEL/+
16 kHz
Mpdz DEL/DEL
40kHz
Mpdz DEL/DEL
90db
85db
80db
75db
70db
65db
60db
55db
50db
45db
40db
35db
30db
25db
20db
nV
mS
E
Sound Pressure Level (dB)
Frequency
8 kHz
16 kHz
32 kHz
40 kHz
****
***
****
****
Mpdz DEL/+ N=22
Mpdz DEL/DEL N=13

Figure 6

Figure 6. Loss of MPDZ leads to tonotopically matching hair bundle and hearing defects in young adults. A) MYO6 labeling of the auditory epithelium at P21 (maximal projection). In spite of severe apical patterning defects in neonates, no HC death is observed in young adults. **B)** GNAI labeling (magenta) at P15 (maximal projection). GNAI signal at stereocilia tips (arrowheads) in control OHCs is lost in *Mpdz* mutant at the cochlear base, but retained at the cochlear apex. In IHCs, GNAI signal is mostly retained at tips even at the cochlear base. **C)** Scanning electron microscopy images of representative OHCs and IHCs at P21 at the cochlear base and apex. Defects include flat and misshapen OHC bundles, and missing or irregular stereocilia placement in the first row in IHCs at the cochlear base. Hair bundle morphology in OHCs and IHCs is relatively normal at the cochlear apex. **D)** Auditory brainstem response (ABR) waveforms at variable sound pressure levels for one control littermate (16kHz) and one *Mpdz* mutant (16 and 40 kHz). The threshold of ABR response is indicated (arrowheads). **E)** ABR thresholds by genotype (8, 16, 32, 40 kHz). Animal were tested between P21 and P25. N = number of animals (two-way ANOVA test with a multiple comparison test; 8kHz: $p<0.0001$ ****; 16kHz: $p<0.001$ ***; 32kHz: $p<0.0001$ ****; 40kHz: $p<0.0001$ ****). A plotted value of 100dB indicates that animals did not respond at 90bD. Scale bars are 10μm (A-B, C for OHCs), 5μm (C for IHCs).

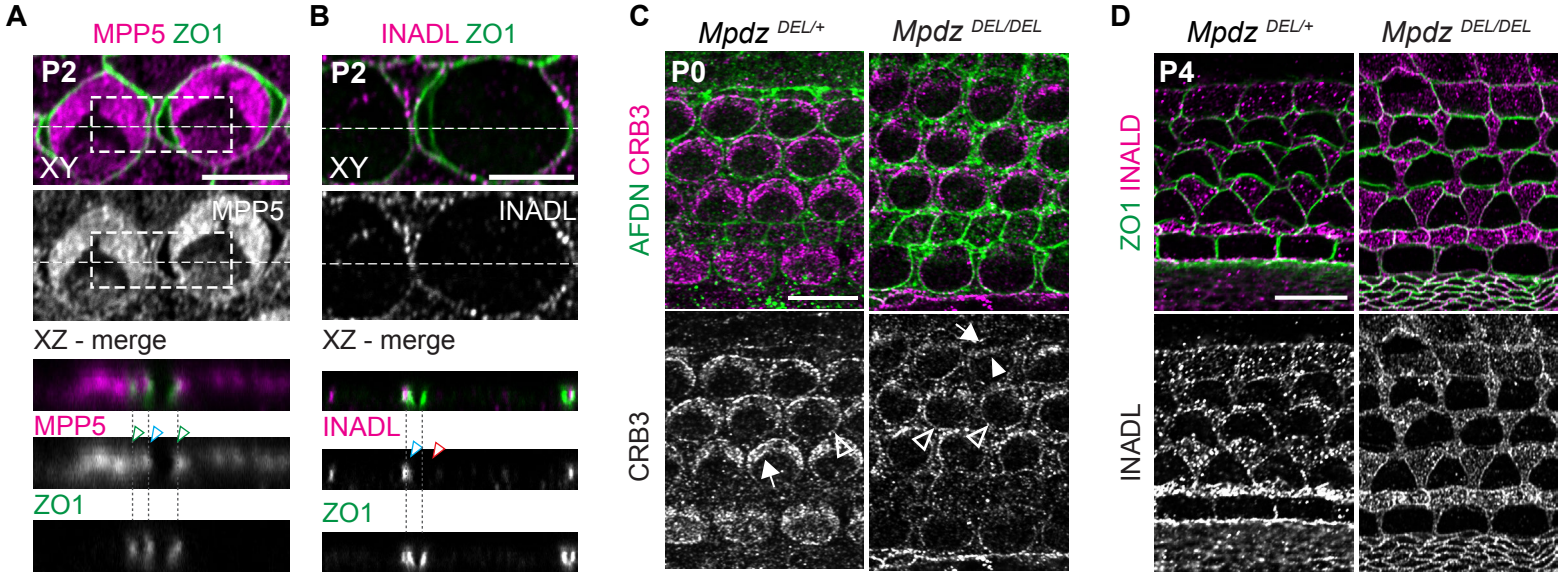

Supp. Figure 1

Supplementary Figures

Supplementary figure 1. MPP5 and INADL are enriched at the apical junction in support cells. MPDZ is required for the correct distribution of CRB3 at the hair cell apical membrane. A-B) Immunolabeling in flat (XY) and projection (XZ) views of two OHC3 at the cochlear mid. We took advantage of TCA fixation artifacts where the apical membrane of the HC and neighboring support cell became separated. MPP5 (A) is enriched at both HCs (green arrowheads) and support cells (blue arrowheads) apical junctions. In contrast, INADL (B) is only enriched at the support cell apical junction (blue arrowhead) and absent at the HC junction (red arrowhead). **C)** CRB3 labeling in P0 *Mpdz* mutant (cochlear base). In absence of MPDZ, CRB3 is lost at the bare zone (arrow) and ectopically found in the hair bundle (solid arrowhead). CRB3 is retained at apical junctions (hollow arrowheads). Note how CRB3 behaves similarly to MPP5 (see Figure 4E-F). **D)** INADL labeling in P4 *Mpdz* mutant (cochlear base). INADL enrichment remains unchanged in absence of MPDZ, as expected from the absence of INADL signal in HCs (B; see also Figure 4D). Scale bars are 10μm.

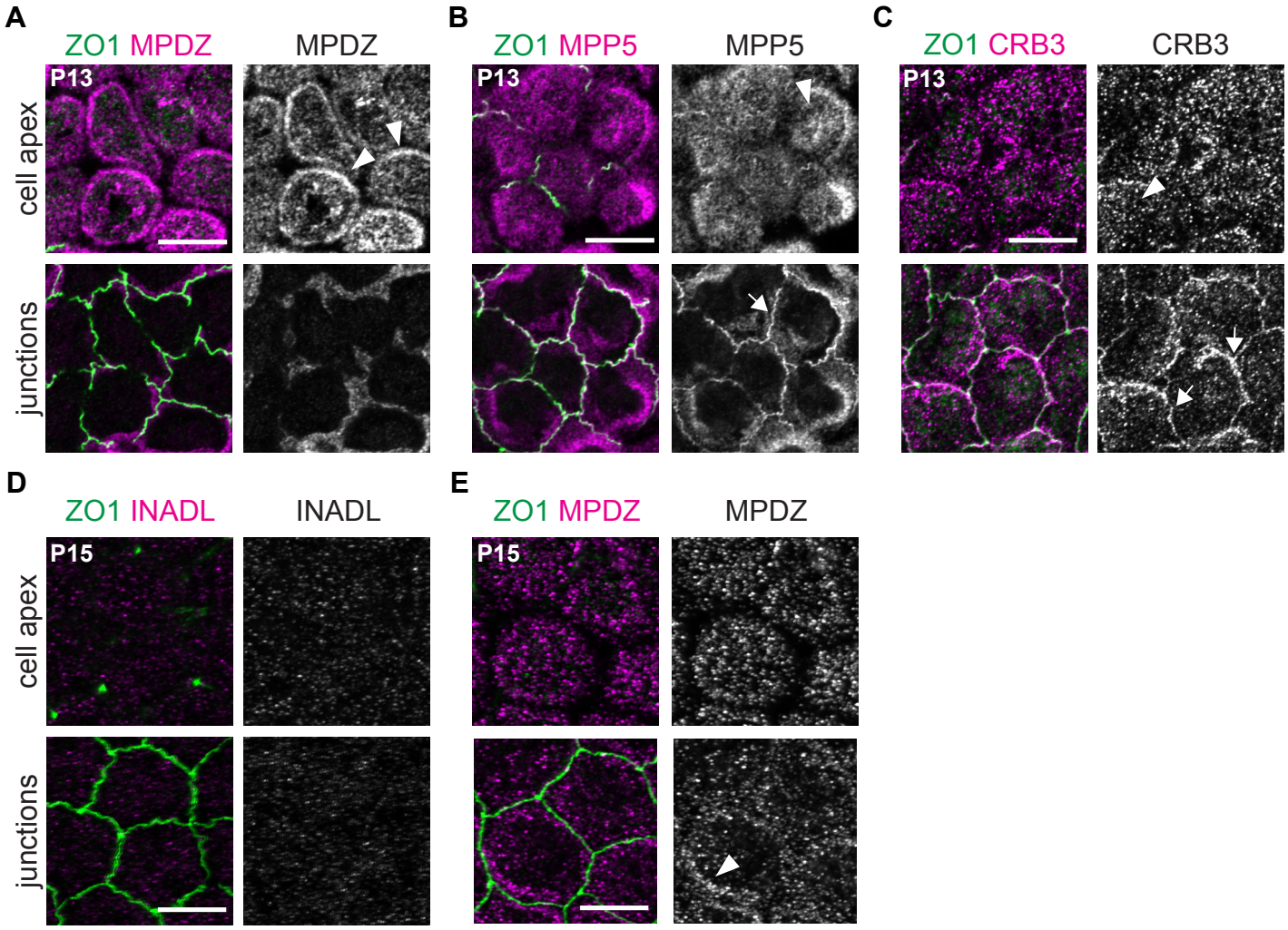

Supp. Figure 2

Supplementary figure 2. MPDZ, MPP5 and CRB3 localization in the epithelium of the hindbrain choroid plexus. A-E) Immunolabeling in P13-P15 wild-type 4th ventricle choroid plexus (projection of a confocal stack) where ZO1 defines the apical junctions. A projection of the most apical Z slices in the stack (1 µm depth) is used to visualize the apical membrane (top panels, “cell apex”). A projection of adjacent, more basal Z slices in the same confocal stack (1 µm depth) is used to visualize the apical junctions (bottom panels, “junctions”). **A)** MPDZ is enriched at the apical membrane where it accumulates near the junctions (arrowheads), but MPDZ is not itself co-localized with ZO1 at apical junctions. **B-C)** In contrast, MPP5 (B) and CRB3 (C) occupy the apical membrane like MPDZ (arrowheads), but also colocalize with ZO1 at the apical junctions (arrows). **D)** INADL is not detected either at the apical membrane or at apical junctions in the choroid plexus epithelium. **E)** An independent experiment at P15 confirmed that MPDZ is enriched at the apical membrane where it accumulates near the junctions (arrowheads), but MPDZ is not itself co-localized with ZO1 at apical junctions. Scale bars are 10µm.

	Our Data	Feldner et al., EMBO Mol Med 2017		Yang et al., EMBO Mol Med 2019
Mpdz mouse allele	*Mpdz em1(IMPC)J/Mmucd*	*MpdzΔ*	*Mpdz Gt(XG734)Byg* (From Milner et al, Addict Biol 2015)	
exons targeted and protein truncation	indel in exon 6 > truncation after 1st PDZ domain	floxed exons 4-5 > truncation before all 13 PDZ domains	gene trap in exons 11-12 > truncation after 3rd PDZ domain	
background	C57BL/6N	C57BL/6 (substrain unknown)	C57BL/6 (substrain unknown)	C57BL/6J
hydrocephalus	not observed	seen by P21	from P3	from P4
survival rate of homozygotes	no death	median 25 days	median 20 days	21 days
frequency of homozygote obtained				
from het x het crosses	genotyping after P21: 20% (N=145)	at birth (P0): 25%	P1 - P10: 20%	at birth (P0): 9%
from het x hom crosses	genotyping from P0 to P21: 43% (N=430)			

Supp. Table 1